Can Tibetan Plateau Snow Depth Influence the Interannual Association between Tropical Indian Ocean Sea Surface Temperatures and Rapidly Intensifying Typhoons?

YUHAO CAI,[a,b,c,d] HAIKUN ZHAO,[a,b,c] PHILIP J. KLOTZBACH,[e] GRACIELA B. RAGA,[f] JING XU,[c] LIGUANG WU,[g] XIANG HAN,[h] BIAN HE,[b] AND JIAN CAO[a]

[a] *Key Laboratory of Meteorological Disaster, Ministry of Education, Joint International Research Laboratory of Climate and Environment Change, Collaborative Innovation Center on Forecast and Evaluation of Meteorological Disaster, Nanjing University of Information Science and Technology, Nanjing, China*
[b] *State Key Laboratory of Numerical Modeling for Atmospheric Sciences and Geophysical Fluid Dynamics, Institute of Atmospheric Physics, Chinese Academy of Sciences, Beijing, China*
[c] *State Key Laboratory of Severe Weather, Chinese Academy of Meteorological Sciences, Beijing, China*
[d] *School of Atmospheric Sciences, Sun Yat-sen University, and Southern Marine Science and Engineering Guangdong Laboratory (Zhuhai), Zhuhai, China*
[e] *Department of Atmospheric Science, Colorado State University, Fort Collins, Colorado*
[f] *Instituto de Ciencias de la Atmósfera y Cambio Climático, Universidad Nacional Autónoma de Mexico, Mexico City, Mexico*
[g] *Department of Atmospheric and Oceanic Sciences and Institute of Atmospheric Sciences, Fudan University, Shanghai, China*
[h] *Ocean College, Zhejiang University, Zhoushan, China*

(Manuscript received 12 September 2022, in final form 8 February 2023)

ABSTRACT: This study finds that the observed decrease in winter–spring Tibetan Plateau snow depth since 2000 has played an important role in weakening the correlation between rapidly intensifying tropical cyclones over the western North Pacific and tropical Indian Ocean sea surface temperatures (SSTs). Tibetan Plateau snow depth modulates convective activity through changes in the South Asian high. Increased Tibetan Plateau snow depth promotes basinwide tropical Indian Ocean cooling in spring through a Gill-type response. In the following seasons, downward latent heat flux anomalies associated with a weaker monsoon circulation contributes to warm SST anomalies over the western tropical Indian Ocean, thus favoring a positive phase of the Indian Ocean dipole. This evolution of tropical Indian Ocean SSTs associated with anomalously high Tibetan Plateau snow depth potentially weakens the relationship between rapidly intensifying tropical cyclone frequency and spring tropical Indian Ocean SSTs. When the effect of Tibetan Plateau snow depth is removed via partial correlation analysis, we find a significant relationship between spring tropical Indian Ocean SSTs and rapidly intensifying tropical cyclones as well as corresponding large-scale environmental factors. The results of this study enhance understanding of changes in tropical cyclone intensity and have implications for seasonal forecasting of tropical cyclone intensity over the western North Pacific basin. This study also emphasizes the importance of Tibetan Plateau thermal forcing in atmosphere–ocean coupling.

KEYWORDS: Sea surface temperature; Tropical cyclones; Climate variability; Snow

1. Introduction

On average, the western North Pacific (WNP) is the most active basin for tropical cyclogenesis, resulting in approximately one-third of the total number of global tropical cyclones (TCs) per year (Schreck et al. 2014). These TCs often bring large economic loss and numbers of casualties for coastal regions in East Asia (Zhang et al. 2009; Lu et al. 2021). Over the past decades, while considerable progress has been made in TC track forecasting, prediction of TC intensity change, in particular where TC intensity increases rapidly [e.g., rapid intensification (RI)], still remains a challenge (Rappaport et al. 2009; DeMaria et al. 2014; Elsberry et al. 2007; Gray 1975; Craig and Gray 1996; Kaplan and DeMaria 2003; Hendricks et al. 2010; Kaplan et al. 2015; Lee et al. 2016). Improved understanding of RI may lead to improved mitigation of TC-related disasters.

Several studies have focused on rapidly intensifying TC (RITC) frequency in response to climate variability on various time scales (Wang and Zhou 2008; Chunzai Wang et al. 2017; Zhao et al. 2018; Gao et al. 2020; Cai et al. 2022). In general, RITCs over the WNP basin are more prevalent during late boreal summer (hereafter, summer) through boreal autumn (hereafter, autumn), with a peak in September (Wang and Zhou 2008; Shi et al. 2019). On interannual time scales, RITC frequency over the WNP basin has a strong negative relationship with El Niño–Southern Oscillation (ENSO) (Wang and Zhou 2008; Guo and Tan 2018, 2021; Shi et al. 2019). More RITCs occur over the southeastern portion of the WNP during El Niño developing years, primarily due to atmospheric–oceanic conditions becoming more TC favorable in this region during El Niño. Guo and Tan (2018) found that the location of

Supplemental information related to this paper is available at the Journals Online website: https://doi.org/10.1175/JCLI-D-22-0697.s1.

Corresponding author: Haikun Zhao, zhk2004y@gmail.com, haikunzhao@nuist.edu.cn

DOI: 10.1175/JCLI-D-22-0697.1

RI occurrence tends to shift westward due to an eastward advection of ocean heat content during short-duration El Niño–decaying years compared to during long-duration El Niño–decaying years. In addition to ENSO, other studies have focused on how WNP RITC activity is modulated by subtropical Pacific SSTs as well as SSTs in other basins. A positive phase of the Pacific meridional mode (PMM) was shown to trigger a westward Gill-type Rossby wave pattern (Gill 1980) favoring both stronger TCs as well as RI occurrence (Gao et al. 2018).

On decadal or longer time scales, changes in tropical Pacific climate and shifting ENSO conditions have been observed. El Niño events have tended to have their maximum amplitude in the central equatorial Pacific in recent years, and a cool Pacific decadal oscillation (PDO) phase has predominated since the 1990s. Central Pacific El Niño events tend to impact RI duration, while eastern Pacific El Niño events impact RI occurrence (Guo and Tan 2021). Correspondingly, there is a significant decadal change in the ratio of RITCs (Zhao et al. 2018) and an increase in RI events since the late 1990s over the WNP basin (Wang et al. 2015; Song et al. 2020). Decadal to interdecadal changes have also been observed in the interannual correlation between RI and ENSO (Wang and Liu 2016). Changes in RI activity are found to be consistent with phase shifts in the PDO, with increased RI activity in the cool phase of the PDO.

The Tibetan Plateau, referred to as "Earth's third pole," exerts a profound effect on local and global climate and weather events via thermal forcing (Ding 1992; Yanai et al. 1992; Wu et al. 1997, 2007, 2012b; Wang et al. 2008; Lu et al. 2018; Y. Liu et al. 2020). Snow cover over the Tibetan Plateau alters the spatial pattern of diabatic heating through changes in albedo and via hydrological effects (Barnett et al. 1989; Shinoda et al. 2003). These changes then lead to local and remote impacts on climate and weather events, including TCs (Yasunari et al. 1991; Ose 1996; Zhang and Tao 2001; Zhang et al. 2004; Zhu et al. 2015; Li et al. 2018; S. Liu et al. 2020). For example, changes in Tibetan Plateau snow cover during the prior boreal winter (hereafter, winter) and boreal spring (hereafter, spring) can affect the Asian summer monsoon circulation by altering the land–sea thermal contrast and thus rainfall over East Asia (Blanford 1884; Zhang and Tao 2001; Yu and Hu 2008; Si and Ding 2013; Turner and Slingo 2011; Xiao and Duan 2016). Tibetan Plateau snow cover can also trigger a wave train crossing the Pacific, thus impacting surface temperatures in North America (Lin and Wu 2011; Qian et al. 2019; Wang et al. 2020). Several studies have also suggested that Tibetan Plateau snow forcing can affect WNP TC activity via changing atmospheric–oceanic conditions (Xie et al. 2005; Xie and Yan 2007; Zhan et al. 2016; Han et al. 2021; Cai et al. 2022).

Both observational and numerical studies have revealed that SSTAs over various basins can interact with the thermal effects of the Tibetan Plateau (Sun et al. 2019; Liu et al. 2014; He et al. 2018; Wang et al. 2019; Y. Liu et al. 2020; Wang et al. 2020; Zhao et al. 2021). Wang et al. (2019) indicated that Tibetan Plateau thermal forcing could anomalously cool SSTs over the tropical Indian Ocean (TIO) via modulation of the monsoon circulation. Monsoonal convection is, in turn, suppressed by cold TIO SSTs. As a capacitor, TIO SST warming typically follows a mature El Niño event through an "atmospheric bridge" mechanism (Klein et al. 1999; Xie et al. 2002), subsequently exciting a Kelvin wave propagating into the western Pacific and a so-called discharging process (Xie et al. 2009). This process can significantly decrease WNP TC genesis frequency by enhancing an anticyclonic circulation, suppressing convection, and increasing vertical wind shear (Du et al. 2011; Zhan et al. 2011a,b; Wang et al. 2021; Liu et al. 2021). Nevertheless, the extent of the influence of TIO SST on WNP TC activity varies due to other forcing sources. As suggested by previous studies (Ha et al. 2014; Zhan et al. 2014; Huangfu et al. 2019; Liu et al. 2019), the limited impact of TIO SST on WNP TC activity may depend on the specific configuration of Pacific SSTAs.

One recent study (Cai et al. 2022) showed that air–sea feedback over the subtropical eastern Pacific, that is, the feedback of a PMM-like SST mode, provides a bridge connecting interannual variability in Tibetan Plateau snow depth with WNP RITC frequency. Anomalous Tibetan Plateau snow depth can trigger PMM-like SSTAs in the following seasons, thus enhancing the correlation between summer–autumn WNP RITC frequency and prior winter–spring Tibetan Plateau snow depth after 2000 (Fig. 2 and Fig. S2 in the online supplemental material) (Cai et al. 2022; Gao et al. 2018). However, the seasonal TIO SST evolution associated with Tibetan Plateau snow depth and its influence on WNP RITCs remain unclear. A statistical analysis by Gao et al. (2020) indicated that warm SSTAs over the TIO can significantly increase the proportion of RITCs to the total TCs number over the WNP, due to a local large ocean heat content. However, they found no significant change in RITC frequency.

Given the aforementioned feedback between Tibetan Plateau thermal forcing and TIO SST, we focus on the impact of Tibetan Plateau snow depth on the evolution of TIO SST and its subsequent impact on WNP RITC frequency. We also attempt to provide a plausible reason for why spring TIO SST anomalies are not significantly related to RITC frequency since 2000. The remainder of this study is arranged as follows. Section 2 describes the data and methodology used. Section 3 presents the statistical relationship between Tibetan Plateau snow depth and RITC frequency and the evolution of Indo-Pacific SSTAs. The role of Tibetan Plateau snow depth in weakening the relationship between TIO SST and RITC frequency is examined in section 4, while section 5 discusses the physical mechanism of TIO SST evolution in response to higher Tibetan Plateau snow depth. A summary and discussion are given in section 6.

2. Data and methods

a. TC and atmospheric and oceanic data

TC best-track data are derived from the Joint Typhoon Warning Center (JTWC; Chu et al. 2002). All TCs ≥ 34 kt (~17.2 m s^{-1}; 1 kt ≈ 0.51 m s^{-1}) during the peak season from July to November in the WNP are considered in this study. July–November TC frequency over the WNP basin shows striking interannual variability and a significant decreasing

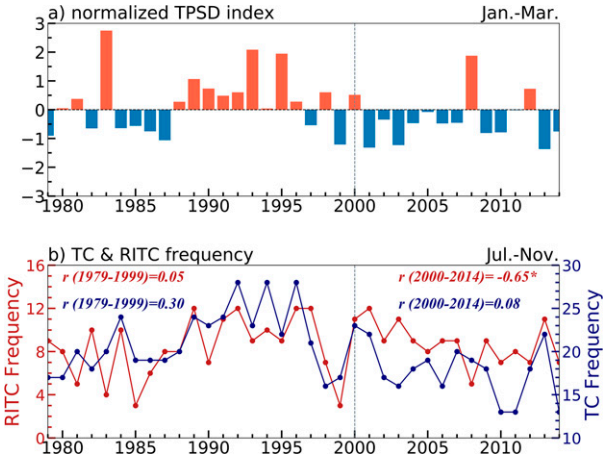

FIG. 1. Time series of (a) the normalized Tibetan Plateau snow depth index (bars) from January to March of 1979–2014, (b) July–November TC genesis frequency (blue line), and RITC frequency (red line) from 1979 to 2014. The correlation coefficient (r) between Tibetan Plateau snow depth in (a) and TC genesis frequency (blue text) and RITC frequency (red text) during the first subperiod (left) and second subperiod (right) are shown at the top of (b). The asterisk denotes statistical significance at the 90% confidence level.

trend since the late 1990s (Fig. 1b), as also shown in previous studies (Liu and Chan 2013; Hsu et al. 2014; Zhao and Wang 2016; Zhao et al. 2018).

Monthly atmospheric fields are obtained from the NCEP–Department of Energy AMIP-II reanalysis, with a 2.5° × 2.5° horizontal resolution and 17 vertical pressure levels (Kanamitsu et al. 2002). Monthly SSTs are obtained from the National Oceanic and Atmospheric Administration's Extended Reconstructed Sea Surface Temperature, version 5, with a horizontal resolution of 2.0° × 2.0° (Huang et al. 2017). Monthly outgoing longwave radiation (OLR) data are derived from NOAA (Liebmann and Smith 1996), and monthly precipitation data are obtained from the Global Precipitation Climatology Project (Adler et al. 2018).

b. Definition of rapidly intensifying tropical cyclones

Rapid intensification has been defined in several studies to be an increase in maximum sustained surface wind speed of ≥30 kt or a decrease in minimum sea level pressure of at least 42 hPa over a 24-h period (Kaplan and DeMaria 2003; Holliday and Thompson 1979; Brand 1973; Ventham and Wang 2007; Wang and Zhou 2008). In this study, we adopt the definition of RITCs used by Wang and Zhou (2008). The following criteria for RI must be satisfied: 1) an increase of at least 5 kt in the first 6 hours; 2) an increase of at least 10 kt in the first 12 hours; and 3) an increase of at least 30 kt in the first 24 hours. A TC is considered an RITC if it undergoes RI at least once during its lifetime.

Given our RI and TC definitions, a total of 923 TCs, including 373 RITCs, occurred over the WNP during July–November from 1979 to 2014. The genesis locations of all WNP TCs are displayed in Fig. S1a. Tropical cyclones typically form near the monsoon trough, that is, the convergent zone between southwesterly flow and easterly trade wind flow. Consistent with Zhao et al. (2018), the formation location of WNP RITCs tends to occur more southward and eastward compared to non-RITCs. Moreover, RI occurrence tends to concentrate in the latitudinal zone from 7° to 20°N, where weak vertical wind shear, high midlevel humidity, and high TCHP are favorable for TC intensification (Fig. S1b). Hence, following Cai et al. (2022), we classify the off-equatorial WNP (7°–20°N, 120°–170°E) as the TC main development region, where ~76% of RITCs and ~72% of RITCs experiencing at least one RI episode form (Fig. S1b). Throughout the remainder of the paper, we calculate WNP RITC frequency during July–November (i.e., the peak TC season) unless otherwise noted.

c. Tibetan Plateau snow depth index

Monthly snow depth data are obtained from the Global Land Data Assimilation System (GLDAS; Rodell et al. 2004). These data are available at a 1° × 1° horizontal resolution and cover the region bounded by 60°S–90°N, 0°–360°. The thermal effect of snow is characterized by its regional dependence over the Tibetan Plateau (Li et al. 2001; Chenghai Wang et al. 2017; Wang et al. 2019). In this study, we examine the impact of snow depth over the eastern part of the Tibetan Plateau on both TIO SST evolution and WNP RITC frequency. The thermal effect of snow over the eastern Tibetan Plateau on global and local climate has been widely investigated (Lin and Wu 2011; Lyu et al. 2018; Wang et al. 2020; Han et al. 2021; Cai et al. 2022). Following our previous work (Cai et al. 2022), the Tibetan Plateau snow depth index is defined to be the area-averaged snow depth from the GLDAS over the eastern Tibetan Plateau (28°–40°N, 90°–105°E). We evaluate changes in snow depth over the Tibetan Plateau during the latter part of the winter and the early part of the spring [January–March (JFM)]. The time series of JFM Tibetan Plateau snow depth extends from 1979 to 2014 and shows an enhanced correlation with RITC frequency since 2000 (Fig. S2). Also, in agreement with previous studies (Si and Ding 2013; Zhu et al. 2015; Chu et al. 2018; You et al. 2020; Cai et al. 2022), the Tibetan Plateau snow depth index shows a strong downward trend since 2000 (Fig. 1a). Unless otherwise noted, when we discuss Tibetan Plateau snow depth, we are referring to eastern Tibetan Plateau snow depth during JFM.

As the GLDAS dataset of Tibetan Plateau snow depth ends in 2014, we extend the length of the Tibetan Plateau snow depth time series using other reanalysis datasets. The significantly increased interannual relationship between RITC frequency and Tibetan Plateau snow depth using GLDAS can also be found using Tibetan Plateau snow depth from ERA-Interim (Dee et al. 2011) and JRA-55 Reanalysis (Kobayashi et al. 2015) datasets when extending these datasets to 2018 (Fig. S2) (Cai et al. 2022). However, when Tibetan Plateau snow depth from ERA5 (Hersbach et al. 2020) is examined, we find a weak increase in the interannual relationship between RITC frequency and Tibetan Plateau snow depth since the late 1990s (Fig. S2). This lack of relationship using ERA5 snow depth data may be due to the fact that ERA5 does not

assimilate Interactive Multisensor Snow and Ice Mapping System snow data at high altitudes (Orsolini et al. 2019). More importantly, Tibetan Plateau snow depth derived from GLDAS compares well with changes in 2-m temperature over the eastern Tibetan Plateau from ERA-Interim and JRA-55 Reanalysis datasets (Fig. S3), which enhances our confidence in their representation of Tibetan Plateau snow depth. To further enhance the reliability of the Tibetan Plateau snow depth index from GLDAS, we also use observed snow depth data from 1979 to 2013 as recorded by 102 meteorological stations. The observation snow depth dataset, provided by the National Meteorological Information Center and Tibet Meteorological Bureau (2018) can be downloaded from the National Tibetan Plateau Data Center (https://data.tpdc.ac.cn/en/data/72d6dadf-8e1c-458b-b24e-91539042dfe6/). In this study, we only select station data located in our eastern Tibetan Plateau region to derive the Tibetan Plateau snow depth index. As expected, there is a significantly increased relationship around 2000 when using in situ data calculated using a sliding correlation (red line in Fig. S2). The Tibetan Plateau snow depth index from in situ observational snow data shows a poorer correlation with 2-m temperature over the eastern Tibetan Plateau than that from GLDAS (Fig. S3d). Consequently, we choose to use the GLDAS dataset as a direct extension of our previous study (Cai et al. 2022).

d. Oceanic indices

Both the tropical Indian Ocean basin mode (TIOB) and Indian Ocean dipole (IOD) mode's influence on RITC frequency over the WNP basin are considered in this study. The TIOB index is defined as SSTAs averaged over the tropical Indian Ocean (20°S–20°N, 40°–110°E), following the definition used in Xie et al. (2009). The IOD is defined as the SSTA difference between the eastern Indian Ocean (10°S–0°, 90°–110°E) and the western Indian Ocean (10°S–10°N, 50°–70°E) [dipole mode index (DMI)] (Saji et al. 1999).

Both the Niño-3.4 index and the El Niño Modoki index (EMI; Ashok et al. 2007) are used in this study. The Niño-3.4 index is calculated using the three months that typically characterize the mature phase of ENSO (December–February). The EMI is calculated following Ashok et al. (2007):

$$\mathrm{EMI} = \mathrm{SSTA}_C - 0.5 \times \mathrm{SSTA}_E - 0.5 \times \mathrm{SSTA}_W,$$

where SSTA_C, SSTA_E, and SSTA_W represent the area-mean SST anomaly averaged over the central Pacific (SSTA_C:10°S–10°N, 165°E–140°W), the eastern Pacific (SSTA_E:15°S–5°N, 110°–70°W), and the western Pacific (SSTA_W:10°S–20°N, 125°–145°E), respectively.

The PMM SST index describes the SSTA gradient between the subtropical and equatorial eastern Pacific (Chiang and Vimont 2004). All oceanic indices other than the Niño-3.4 index are evaluated from JFM through the TC season to examine the SST evolution in response to changes in JFM Tibetan Plateau snow depth.

e. Significance test

We use a two-tailed Student's test to examine statistical significance of correlation and regression coefficients as well as composites. Unless stated otherwise, significance is evaluated at the 90% confidence level ($p \leq 0.10$).

f. Numerical experiments

We use the NCAR Community Earth System Model, version 1.2.2 (CESM1.2.2), to verify the physical mechanism of how Tibetan Plateau snow depth–related SSTAs over the TIO modulate the atmospheric circulation. CESM is a state-of-the-art Earth system model, with interactive atmosphere, ocean, sea ice, and land components (Hurrell et al. 2013; Neale et al. 2010). The model experiments in this study are implemented with the F2000_CAM5 component set at a resolution of 1.9° × 2.5° with 26 hybrid vertical levels. All carbon dioxide, aerosol, solar, and ozone forcings are fixed at their year 2000 values.

We conducted one control experiment and two sensitivity experiments. The control run (CTRL) was forced by the observed climatological mean seasonal cycle of global SSTs. Two other sensitivity experiments (referred to as EXP1 and EXP2) are the same as CTRL but with different SSTA states derived from partial regression analyses (see Table 4), added to climatological mean SSTs in the Indo-Pacific region (15°S–15°N, 60°–150°E). All experiments were run for 30 years, and outputs of the last 20 years are analyzed.

3. Tibetan Plateau snow depth, RITC frequency, and evolution of Indo-Pacific SSTAs

As can be seen in Fig. 1b (blue line), preceding winter–spring Tibetan Plateau snow depth does not correlate significantly with the following peak-season TC genesis frequency over the full period (1979–2014) or for either of the two subperiods (1979–99 and 2000–14). However, the correlation between preceding winter–spring Tibetan Plateau snow depth and the following peak-season RITC frequency since 2000 shows an abrupt increase in significance (red text in Fig. 1b). Tibetan Plateau snow depth insignificantly correlated ($r = 0.05$) with RITC frequency during 1979–99, while the correlation was significant ($r = -0.65$) during 2000–14 (Fig. 1b). These results are consistent with an analysis of the relationship between RITCs and several different snow depth datasets by Cai et al. (2022) (Fig. S2).

In response to higher Tibetan Plateau snow depth during the subperiod from 2000 to 2014, the SSTA pattern (Fig. 2a) is characterized by a negative phase of the PMM and a central Pacific ENSO-like SST pattern. The response to higher Tibetan Plateau snow depth during the 1979–99 subperiod reflects more of an eastern Pacific (EP) ENSO-like SST pattern (Fig. 2b). The Tibetan Plateau snow depth–forced development of the PMM-like and central Pacific ENSO-like SST pattern is further confirmed in Fig. 3c. Cai et al. (2022) highlighted the role of PMM-like SSTAs as being an important connective link between Tibetan Plateau snow depth and boreal summer–autumn WNP RITC frequency. From 2000 to 2014, the synergistic effect of the prevailing jet and the low-frequency SST mode combined with the thermal forcing of the Tibetan Plateau snow depth promoted barotropic gyres responsible for the occurrence of a cold PMM-like SST pattern. Then the cold PMM-like SST pattern triggers anticyclonic flow in the WNP as a Gill-type Rossby wave response, favoring a strong negative correlation between

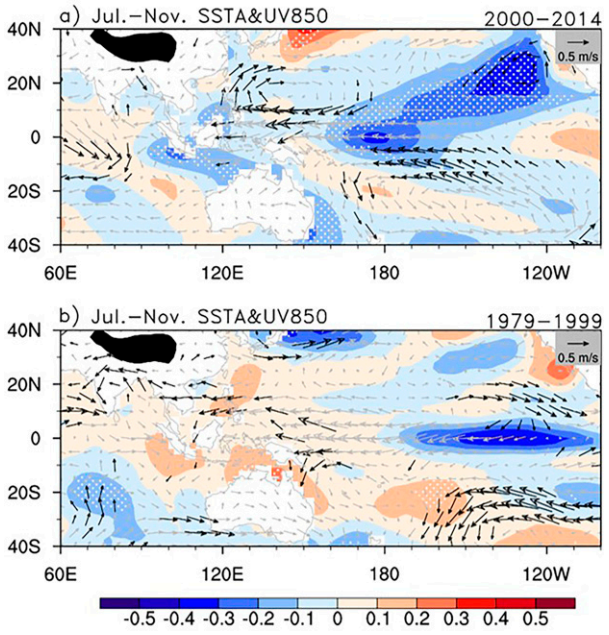

FIG. 2. Regression of 850-hPa wind anomalies (vectors; m s^{-1}) and SSTAs (shading; °C) in the peak season on the Tibetan Plateau snow depth index during (a) 2000–14 and (b) 1979–99. White dots and black arrows indicate that regression coefficients are significant at the 90% confidence level.

Tibetan Plateau snow depth and RITC frequency (Fig. 1b) (Cai et al. 2022; Gao et al. 2018).

Meanwhile, we find an out-of-phase relationship between Tibetan Plateau snow depth and SSTAs over the TIO in the peak season from 2000 to 2014 (Fig. 2a). During 2000–14, significant cold anomalies develop with high Tibetan Plateau snow depth over the eastern Indian Ocean and the South China Sea (SCS) while warm anomalies develop over the western Indian Ocean in the peak season. These SST patterns imply that Tibetan Plateau snow depth potentially impacts IOD development during the peak season. Additionally, when Tibetan Plateau snow depth is higher than normal, basinwide cold anomalies over the TIO occur during the spring (Fig. 3a). The evolution of TIO SSTAs during 2000–14 can also be seen when examining lag correlations between Tibetan Plateau snow depth and the TIOB and DMI indices (Fig. 3b). We find significant negative correlations between preceding winter–spring Tibetan Plateau snow depth and the TIOB index from January to April that become insignificant by summer, with significant positive correlations between preceding winter–spring Tibetan Plateau snow depth and the DMI from May to September.

4. Tibetan Plateau snow depth's role in weakening the TIOB SST–RITC relationship since 2000

a. *TIO SST–RITC frequency relationship*

Gao et al. (2020) suggested that TIO SSTAs significantly correlate with the proportion of RITCs but do not significantly correlate with RITC frequency in the simultaneous season. We find a similar result, with RITC frequency insignificantly correlating with the prior season's TIOB index (Table 1). There is also an insignificant correlation between the spring TIOB index and TC frequency during 2000–14. However, we do find that the correlation over a longer period (1979–2014) is significant. These results are somewhat different from those of Zhan et al. (2011a, 2014), potentially due to interdecadal changes in seasonal TC activity (Choi et al. 2019; Zhao and Wang 2019; Wu et al. 2021). As shown in Table 2, the frequency of TCs and RITCs are both weakly correlated with the January–September (JAS) DMI when the mature IOD typically occurs. These insignificant correlations also exist when using any three-month averaging period of the DMI from May–July to September–November. Most previous studies have focused on the impact of the IOD on TC activity over the TIO (Yuan and Cao 2013; Wahiduzzaman and Yeasmin 2019; Wahiduzzaman et al. 2022), while its impact on WNP TC activity has been less studied (Zhou et al. 2019). Note that the IOD modulation of basinwide WNP TC frequency in the aforementioned studies did not purely reflect its individual effect but, rather, the synergetic effect of IOD and concurrent ENSO conditions (Pradhan et al. 2011; Liu et al. 2019). The weak correlation between WNP TC frequency and the DMI agree well with the results of Wu et al. (2020) (see their Fig. 4), suggesting a limited role of the IOD in controlling WNP TC frequency.

To understand the cause of the weak correlation between the spring TIOB and RITC frequency, we focus on changes in SSTAs and the low-level circulation regressed onto the negative spring TIOB index (with indices multiplied by −1). As shown in Fig. 4, the basinwide TIO SSTA pattern observed in MAM does not typically persist into the peak season. Cold SSTAs occur over the Indo-Pacific in MAM and May–July (MJJ) (Figs. 4a,b), along with latitudinally alternating easterlies and westerlies over the SCS and Maritime Continent when the spring TIOB index is below normal. However, during JAS, significant warm SSTAs begin to cover the western TIO, with the large region of cold SSTAs shrinking and becoming confined to the eastern TIO, SCS, and to the east of the Philippines in JAS and SON (Figs. 4c,d). Only weak anomalous changes are observed in the WNP circulation (Fig. 4d), hinting that there may only be small changes in WNP RITCs. The existence of the SST dipole mode over the TIO and the wind fields (Fig. 4d) over the WNP during autumn indicate a weak correlation between RITC frequency and the DMI from boreal summer to autumn.

b. *Role of Tibetan Plateau snow depth on the evolution of TIO SSTAs*

As noted above, the seasonal evolution of TIO SST from a spring SST pattern characterized by basinwide anomalies of the same sign to an IOD-like SST mode are likely responsible for the weak correlation between spring TIOB and RITC frequency during the peak season from 2000 to 2014. This relationship is likely related to the recent interdecadal decrease in

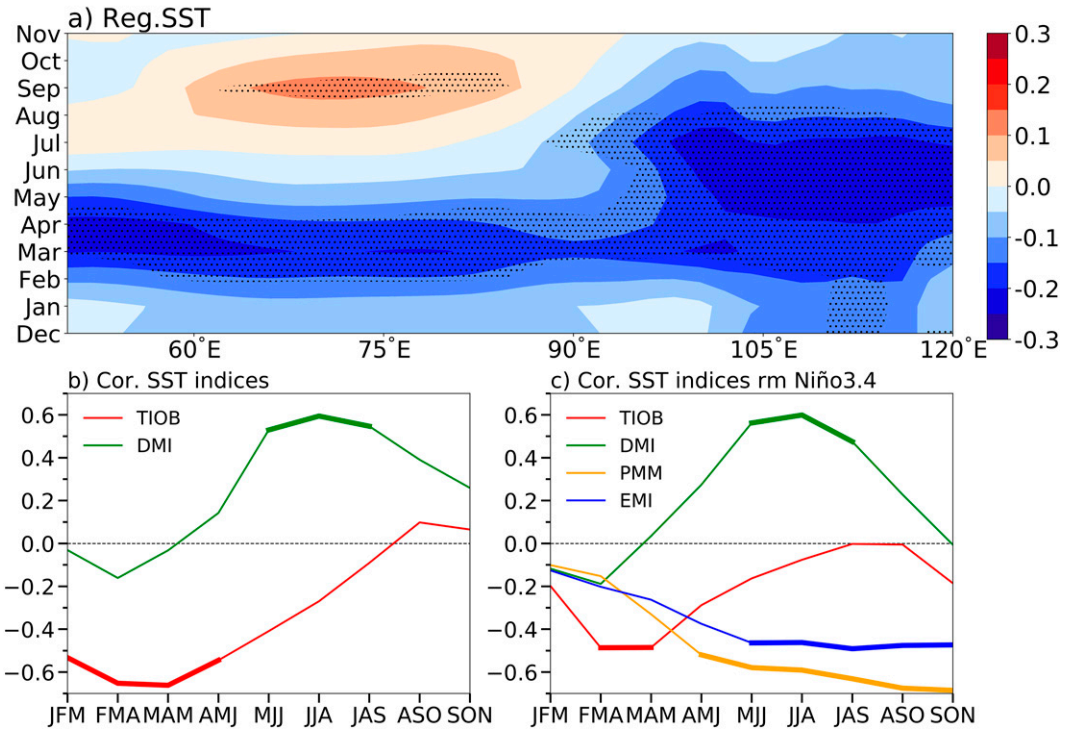

FIG. 3. (a) Time–longitude section of SSTAs (°C) over the TIO (averaged over 5°S–5°N) regressed on the Tibetan Plateau snow depth index from 2000 to 2014. Black dots denote values significant at the 90% confidence level. (b) Lagged correlations of the Tibetan Plateau snow depth index with the TIOB index (red line) and the DMI (green line) from 2000 to 2014. (c) As in (b), but for lagged partial correlations of the Tibetan Plateau snow depth index with four SST indices (and the Niño-3.4 index linearly removed): TIOB index (red line), DMI (green line), PMM index (yellow line), and EMI (blue line) from 2000 to 2014. Thick curves indicate values significant at a 90% confidence level.

Tibetan Plateau snow depth (Fig. 3). Here, we hypothesize that the insignificant correlation between TIO SSTAs and WNP RITC frequency is largely attributed to Tibetan Plateau snow depth forcing. To justify this hypothesis, we calculate the partial correlation coefficient between the TIOB index and RITC counts by linearly removing the Tibetan Plateau snow depth index (Table 3) to investigate the role of Tibetan Plateau snow depth. As expected, the spring TIOB index correlates significantly with the number of RITCs ($r = -0.68$) after linearly removing the Tibetan Plateau snow depth index. The weak correlation with TC genesis frequency also becomes significant when removing the Tibetan Plateau snow depth index (Table 3).

To understand the correlation changes between spring TIOB and RITC frequency after removing Tibetan Plateau snow depth, we linearly remove the Tibetan Plateau snow depth index from all variables via subtraction of the least squares linear fit to the Tibetan Plateau snow depth index. Figures 4e–h display partial regression maps of SSTAs and wind anomalies over the Indo-Pacific onto the negative spring TIOB index with the Tibetan Plateau snow depth linearly removed during 2000–14. Compared with the raw regression maps (Figs. 4a–d), we find an overall similar spatial SST distribution with anomalously cool SSTs predominating over the Indo-Pacific in MAM and MJJ (Figs. 4a,b,e,f). Nevertheless, we do find that cold SSTAs still occupy the western TIO in JAS extending through to SON, with small, insignificant

TABLE 1. Correlations of July–November WNP TCs and RITC frequency with the TIOB index in March–May and in June–August for 1979–99, 2000–14, and 1979–2014, respectively. An asterisk indicates that the correlation is significant at the 90% confidence level.

	TC		RITC	
TIOB index	MAM	JJA	MAM	JJA
1979–99	−0.27	−0.27	−0.11	−0.07
2000–14	−0.41	−0.64*	0.04	−0.32
1979–2014	−0.41*	−0.51*	−0.03	−0.07

TABLE 2. As in Table 1, but for JAS DMI.

DMI	TC	RITC
1979–99	−0.11	−0.14
2000–14	0.00	−0.24
1979–2014	−0.08	−0.16

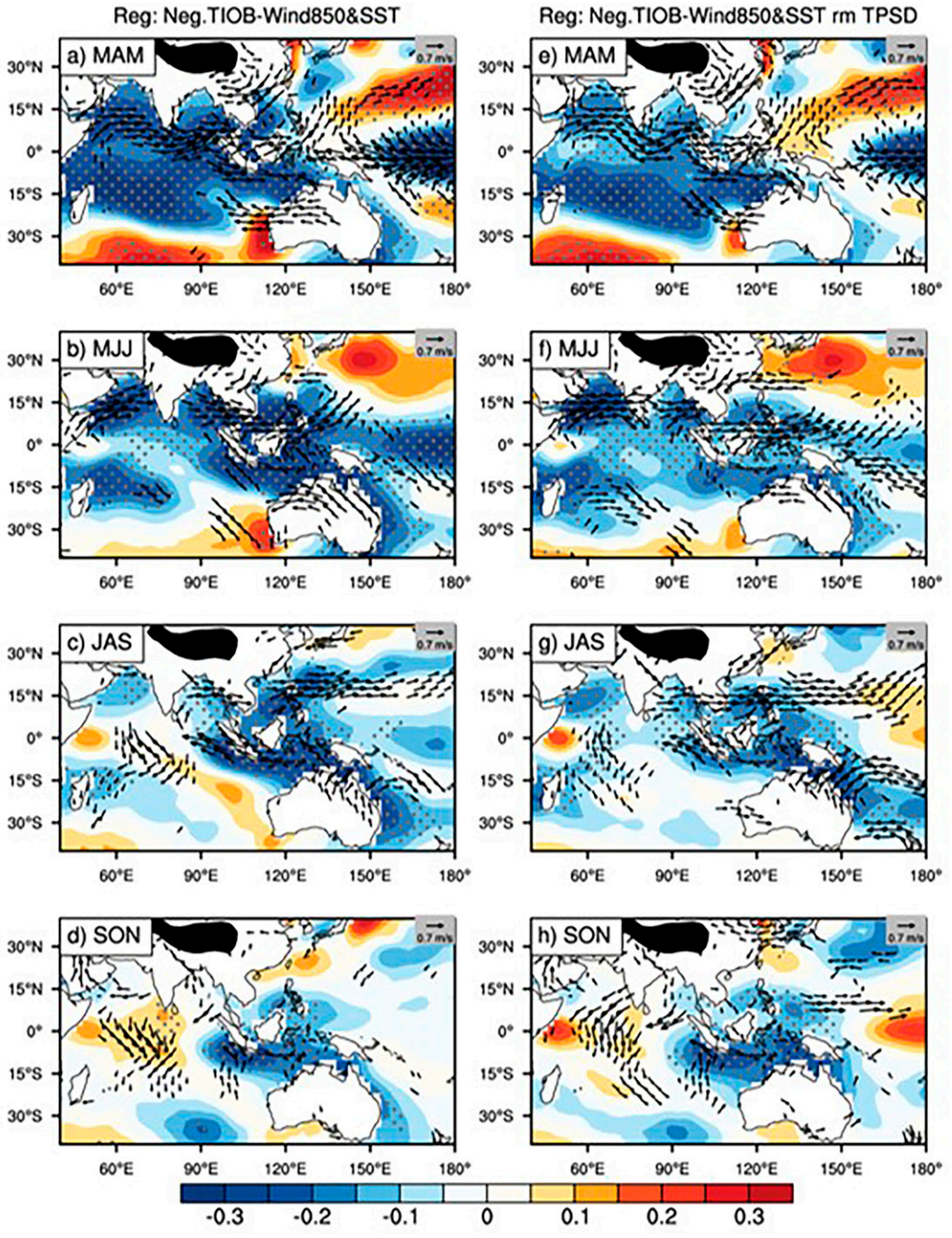

FIG. 4. Regression of (a) MAM, (b) MJJ, (c) JAS, and (d) SON 850-hPa wind anomalies (vectors; m s^{-1}) and SSTAs (shading; °C) on the spring TIOB index (multiplied by −1) during 2000–14. (e)–(h) As in (a)–(d), but for the partial regression with the Tibetan Plateau snow depth index linearly removed. Gray dots indicate values that are significant at the 90% confidence level. Only black vectors at the 90% confidence level are shown.

warm SSTAs occurring over the western TIO (Figs. 4g,h). An anomalous low-level cyclonic circulation develops over the WNP main development region, concurrent with significant cold SSTAs over the eastern TIO and western Pacific (Fig. 4h). The low-level cyclonic circulation over the WNP significantly affects RITCs, thus resulting in a strong relationship between spring TIOB and RITC frequency (Table 3).

The predominant low-level circulation anomaly over the WNP may determine the discrepancy in the relationship between spring TIOB and RITC frequency. When linearly

TABLE 3. Partial correlations of WNP TC and RITC frequency during the peak season with MAM and JJA values of the TIOB index and JAS values of the DMI, respectively, with the Tibetan Plateau snow depth index linearly removed for the period of 2000–14. An asterisk indicates that the correlation is significant at a 90% confidence level.

	TIOB index		DMI
	MAM	JJA	JAS
TC	−0.48*	−0.64*	−0.05
RITC	−0.68*	−0.68*	0.18

removing the Tibetan Plateau snow depth signal, cold SSTAs cover a large region from the eastern TIO to the western Pacific (Figs. 4g,h). Over the equatorial western Pacific, cold SSTAs induce local sinking motion in JAS (Fig. 5c). Correspondingly, significant upward motion occurs in the subtropical WNP, resulting in an anomalous reverse Hadley circulation along with anomalous northerlies in the upper troposphere and southerlies in the lower troposphere. Subsequently, the meridional vertical circulation shrinks north of the equator, while anomalous upward motion is maintained in the subtropical WNP, largely covering the TC main development region (Fig. 5d). The upward motion strengthens the low-level cyclonic flow. These circulation changes together affect RITC activity (Fig. 4h).

Results shown in Figs. 5c and 5d are similar to previous studies (Chen et al. 2018, 2019), which examined how SSTAs over the western Pacific contribute to changes in the Hadley circulation. Additionally, cold eastern TIO SSTAs can also enhance cyclonic flow via eastward propagation of Kelvin waves (Zhan et al. 2011a,b, 2014). When considering the Tibetan Plateau snow depth signal (Figs. 5a,b), although there is a significant inverse Hadley circulation anomaly in JAS, the meridional vertical circulation is weaker than that obtained using partial regression. The anomalous upward motion and anomalous cyclonic flow also disappear in the TC main development region during autumn (Figs. 4c,d). These circulation changes may be caused by anomalous warming of SSTAs in the western TIO (Figs. 4c,d). The impact of warm SSTAs in the western TIO would counteract the cyclonic anomalies induced by cold SSTAs via excitation of easterly Kelvin waves (Gao et al. 2020), leading to a reduction of wind anomalies over the WNP and an insignificant relationship between spring TIOB and RITC frequency (Table 2). Cold SSTAs over the eastern TIO–western Pacific do have an effect, since the warm SSTAs over the western TIO are mostly removed when linearly removing the Tibetan Plateau snow depth signal, contributing to an anomalous cyclonic circulation (Fig. 4h) and thus a strong relationship between spring TIOB and RITC frequency (Table 3).

Regression analyses with and without the Tibetan Plateau snow depth signal indicate that the occurrence of WNP wind

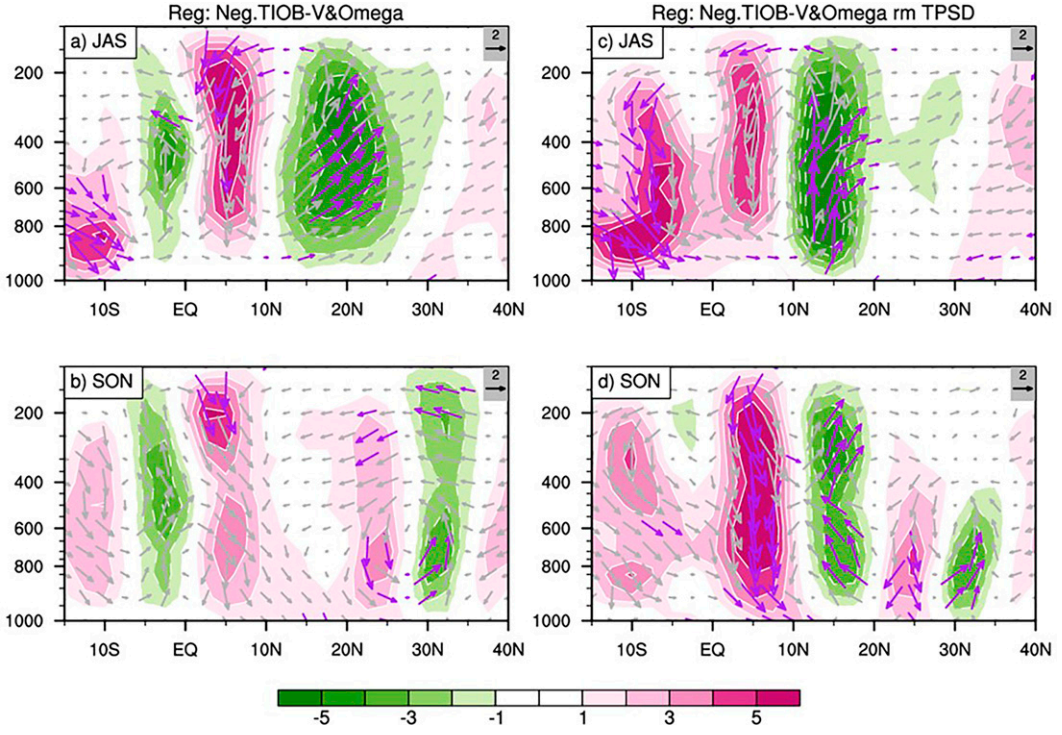

FIG. 5. Regression of the (a) JAS and (b) SON meridional and vertical circulation anomalies (vectors; m s^{-1} for horizontal velocity and -10^{-3} Pa s^{-1} for omega) on the spring TIOB index over the western Pacific (averaged from 125° to 150°E). Shading indicates vertical velocity (10^{-3} Pa s^{-1}). (c), (d) As in (a) and (b), but for the partial regression with the Tibetan Plateau snow depth index linearly removed. Purple vectors denote values significant at a 90% confidence level.

TABLE 4. Design of CESM experiments.

Expt	Design
CTRL	30-yr control run forced by observed climatological SST and sea ice concentration
EXP1	Global climatological SST plus Indo-Pacific monthly SSTAs regressed on a negative spring TIOB index
EXP2	Global climatological SST plus Indo-Pacific monthly SSTAs partially regressed on a negative spring TIOB index while linearly removing Tibetan Plateau snow depth

anomalies may be determined by the amplitude of warm SSTAs over the western TIO (Figs. 4c,d,g,h). To further verify this, we designed two sensitivity experiments listed in Table 4. One (EXP1) is prescribed with regressed August–October (ASO) SSTAs over the Indo-Pacific (15°S–15°N, 60°–150°E) onto negative spring TIOB added to the observed monthly climatological global SST, and the other (EXP2) is the same as EXP1 but for partially regressed SST while linearly removing the Tibetan Plateau snow depth signal. Monthly regressed SSTAs for the two sensitivity experiments are shown in Fig. S4. Consistent with Fig. 4, as expected, EXP1 features a rapid transformation to a positive IOD, while EXP2 shows a slow SST transition. In EXP2, cold SSTAs occur over the Indo-Pacific during August–September, with weak warm SSTAs in the western TIO during October.

Relative to the CTRL experiment, both sensitivity experiments (Figs. 6a,b) have enhanced TIO easterlies, primarily due to the zonal SST gradient (Lindzen and Nigam 1987). In EXP1, western TIO warm SSTs are associated with relatively weak, low-level circulations in the WNP (Fig. 6a). While in response to EXP2, where there is a slow transition to weak, warm SSTAs in the western TIO, an anomalous cyclone is simulated in the subtropical WNP (Fig. 6b), resembling the partial regression pattern shown in Fig. 4h. As expected, a large, anomalous WNP anticyclone occurs in the EXP1 minus EXP2 experiment (Fig. 6c), likely due to warm western TIO SSTAs (Figs. S4b,c). The anticyclone in the EXP1 and EXP2 difference experiment is responsible for offsetting the cyclonic circulation (Fig. 6b), thus leading to disorganized wind field anomalies as shown in Fig. 6a. The model output largely verifies the regression results.

Cold SSTAs from spring through the TC peak season can impact the atmospheric circulation, and thus RITC activity, by exciting Kelvin waves and modulating the Hadley circulation. However, given the close connection between Tibetan Plateau snow depth and basinwide TIO SSTAs in the spring and IOD-like SSTAs in JAS, warm SSTAs begin to develop during late summer, rapidly transitioning into an IOD-like SSTA mode. These anomalies likely reduce the cyclonic flow over the TC main development region, thus weakening the modulation of RITCs by the spring TIO SST during 2000–14. Also, higher Tibetan Plateau snow depth potentially leads to an anticyclonic circulation anomaly over the WNP during the following peak season via negative PMM-like SSTAs (Fig. 2a). The anticyclonic circulation anomaly not only suppresses RITC activity (Cai et al. 2022) but also strongly offsets the impact of cold TIO SSTAs on the WNP circulation.

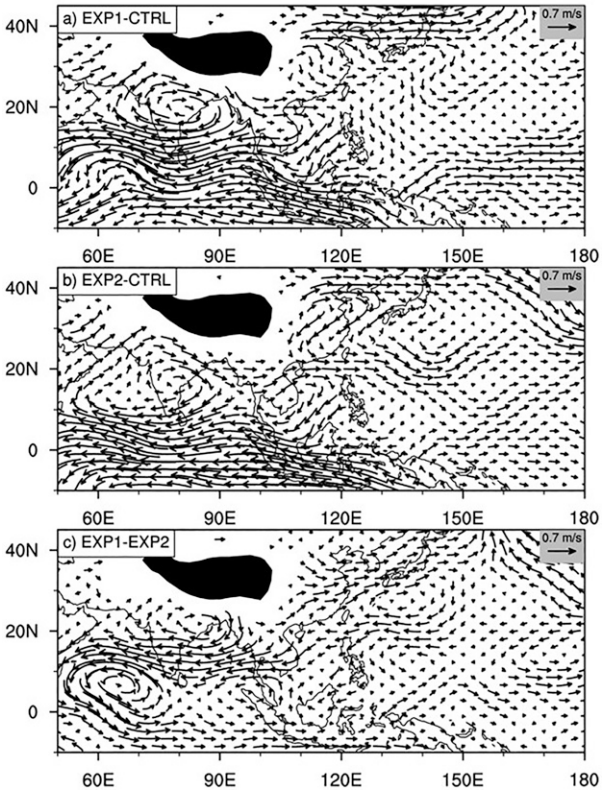

FIG. 6. Simulated atmospheric responses to Indo-Pacific SSTAs forcing. (a) Differences in SON 850-hPa winds (vectors; m s^{-1}) between EXP1 and the CTRL experiment. (b), (c) As in (a), but for differences between EXP2 and the CTRL experiment, and EXP1 and EXP2, respectively.

c. *Changes in large-scale environmental factors*

We find a large increase in the correlation of RITC frequency associated with the TIOB index after linearly removing the Tibetan Plateau snow depth signal. To further show the impact of the spring TIOB on the large-scale environment, we now compare four large-scale environmental factors (low-level vorticity, vertical wind shear, midlevel vertical velocity, and relative humidity) when considering and removing Tibetan Plateau snow depth modulation. Figure 7 shows the regression fields of four environmental factors onto the spring TIOB index with (left column) and without (right column) the Tibetan Plateau snow depth signal. Negative low-level vorticity and an accompanying anomalous anticyclonic circulation corresponding to warm TIO SSTAs extend southward into the TC main development region. Anomalous easterlies and suppressed convection cover most of the TC main development region after removing the Tibetan Plateau snow depth signal (Figs. 7a,c,e,g). The stronger easterly anomalies primarily occur in the southern half of the main development region, leading to an eastward withdrawal of the monsoon

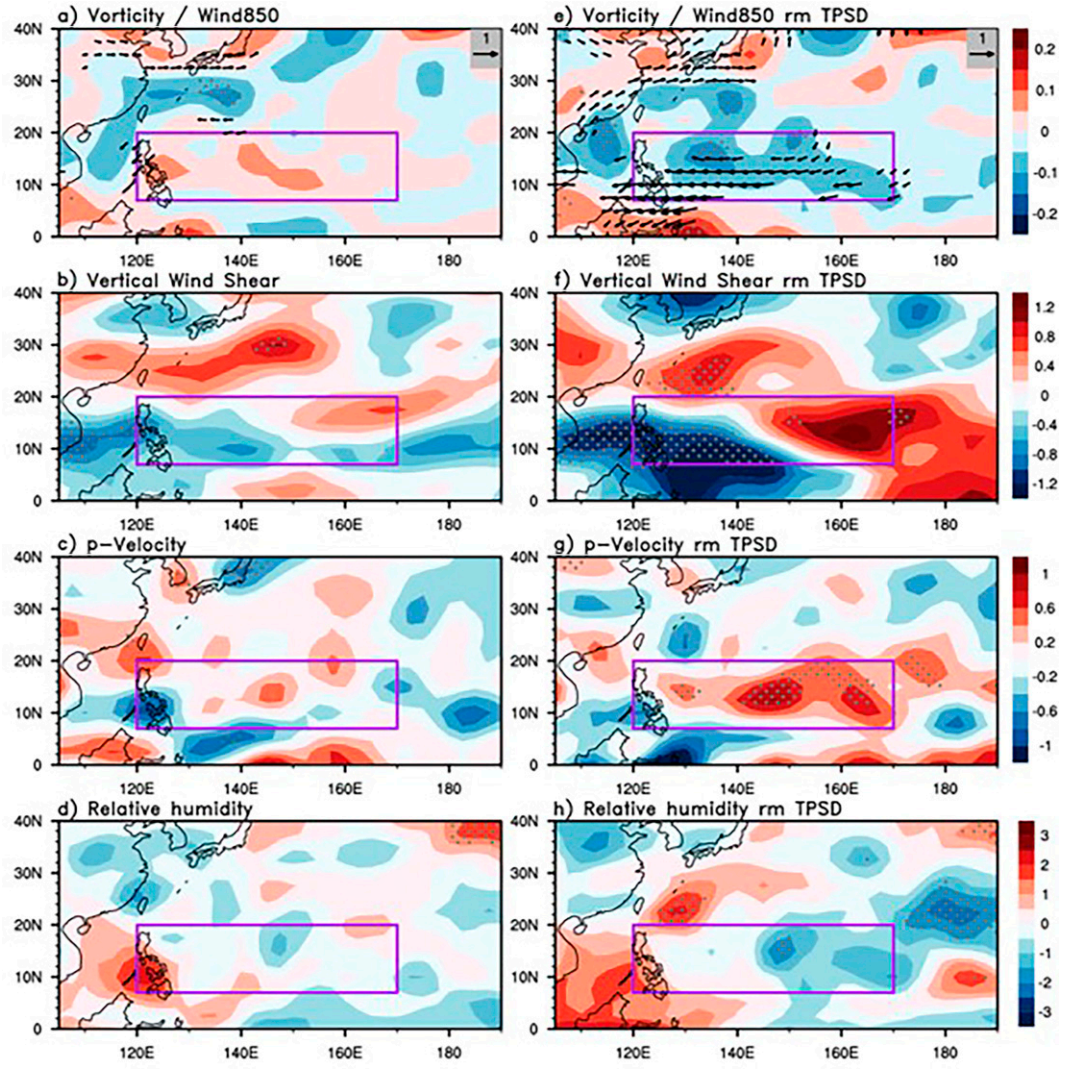

FIG. 7. Regression of several large-scale environment factors during the peak season on the spring TIOB index during 2000–14: (a) 850-hPa relative vorticity (10^{-5} s^{-1}) and winds (vectors); (b) vertical wind shear between 200 and 850 hPa (m s^{-1}); (c) 500-hPa vertical velocity (Pa s^{-1}); (d) 600-hPa relative humidity (%). (e)–(h) As in (a)–(d), but for partial regression with the Tibetan Plateau snow depth index linearly removed. Purple boxes denote the TC main development region. White dots indicate values significant at a 90% confidence level. Black vectors in (a) and (b) denote significance at the 90% confidence level.

trough and weakened convection. All of these conditions are unfavorable for RITCs.

Similar analyses are now performed for the other two factors. Other than negative SCS vertical wind shear anomalies, no significant anomalies are detected in the WNP corresponding to warm spring TIO SSTAs for the raw regression fields (Figs. 7b). After removing the Tibetan Plateau snow depth signal, vertical wind shear anomalies exhibit a remarkable contrast between the eastern and western portions of the TC main development region, with increased positive vertical wind shear east of 150°E (Fig. 7f), mainly contributing to decreased RITC frequency. Negative humidity anomalies increase over the main development region east of 140°E after removing the Tibetan Plateau snow depth signal (Figs. 7d,h).

We also examine the regression of tropical cyclone heat potential (TCHP) to identify the oceanic thermal response (Fig. S5). Both regression maps display negative anomalies over the northeastern portion of the main development region, but their magnitudes in the partial regression map (i.e., filtering the Tibetan Plateau snow depth signal) are smaller than that in the raw regression map, implying that TCHP plays a limited role in supporting the relationship between spring TIO SST and RITC frequency. The significant positive TCHP anomalies related to warm TIO SSTAs tend to increase but are confined within the SCS after removing the Tibetan Plateau snow depth signal. Anomalously high TCHP combined with negative vertical wind shear anomalies indicate that spring TIO SSTAs may favor RITCs in the SCS.

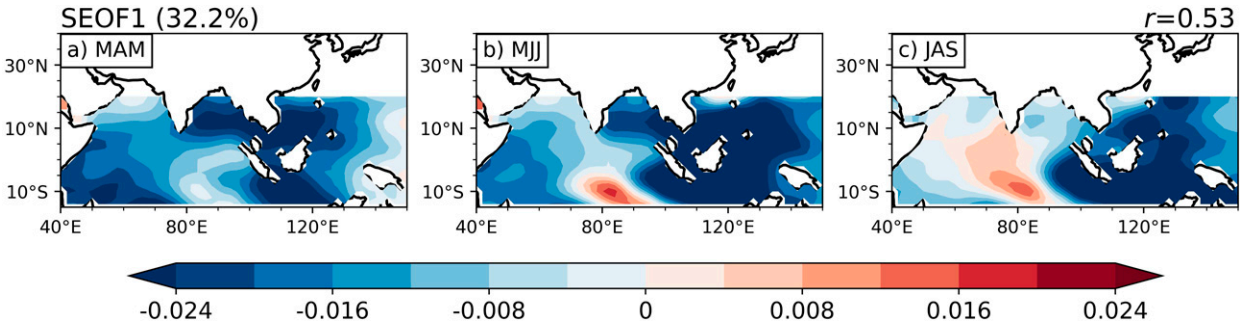

FIG. 8. Spatial patterns of the first seasonal EOF (SEOF) mode of SSTAs over the Indo-Pacific. SSTAs in (a) MAM, (b) MJJ, and (c) JAS while removing the linear fit of the Niño-3.4 index are merged into a sequence matrix over the Indo-Pacific during 2000–14. This mode is well separated from other modes (North et al. 1982). The percentage in parentheses denotes the explained variance. The correlation displayed is between the corresponding PC1 and the JFM TPSD index during 2000–14.

5. Physical mechanism of TIO SST evolution in response to changes in Tibetan Plateau snow depth

In section 4, boreal spring, basinwide cold SSTAs showed limited impact on RITCs possibly due to the development of warm SSTAs over the western TIO during the following season during 2000–14. This evolution of TIO SST has been noted in a recent study (M. Zhang et al. 2022), suggesting a transition from the preceding winter negative TIOB mode to a positive IOD mode in the following peak season. We next conducted season-reliant empirical orthogonal function (SEOF; Wang and An 2005) analysis to capture TIO SST evolution focusing on the period from 2000 to 2014, following M. Zhang et al. (2022). As shown in Fig. 8, the first leading SEOF mode shows a basinwide anomaly pattern in spring that transitions into a dipole mode during the summer, accounting for ~32% of the variance. The spatial pattern of the first SEOF mode resembles the pattern shown in Figs. 4a–d, confirming the greater importance of warming in the western TIO in the spring to summer SST evolution. The principal component series of the first SEOF mode and the Tibetan Plateau snow depth index correlates significantly ($r = 0.53$), but the first SEOF mode correlates insignificantly with RITC frequency ($r = 0.1$). This indicates that the TIO SST evolution pattern and its weak connection with RITC frequency are associated with changes in Tibetan Plateau snow depth forcing.

In this section, we focus on the potential mechanism responsible for TIO SST evolution given Tibetan Plateau snow depth changes. We begin our analysis by excluding the ENSO teleconnection (Klein et al. 1999; Xie et al. 2002; Zhao et al. 2022), due to the significant negative correlation between Tibetan Plateau snow depth and the Niño-3.4 index after 2000 (Wang et al. 2020, 2022). The partial correlation time series of the DMI (removing the Tibetan Plateau snow depth signal) resembles the raw correlation evolution, and the relationship between JFM Tibetan Plateau snow depth and the TIOB index remains significant during the spring. There are slightly reduced magnitudes in lag partial correlations and larger reduced magnitudes in simultaneous partial correlations compared with raw correlations (Figs. 3b,c). These results support the relaying effect of Tibetan Plateau snow depth on TIO SST independent of ENSO. In the next section, all variables have the linear fit to the Niño-3.4 index removed.

In agreement with Fig. 3, SSTAs corresponding to higher Tibetan Plateau snow depth exhibit a transition from a basin-scale TIO cooling during spring to a positive IOD-like SST mode during summer and early autumn in 2000–14 (Fig. 9). A linear regression of low-level winds on Tibetan Plateau snow depth highlights TIO SSTA forced by the atmosphere (Fig. 9a). Associated with higher Tibetan Plateau snow depth is a significant cyclonic circulation in the western TIO in February–April (FMA). Anomalous easterlies occurring over the Maritime Continent converge with anomalous westerlies over the equatorial Indian Ocean (Fig. 9a). The observed wind distribution resembles a Gill-type response (Gill 1980), with westward propagation of a Rossby wave over the TIO and eastward propagation of a Kelvin wave over the Maritime Continent. The cyclonic circulations together with equatorial easterlies promote cold water upwelling over the TIO SST via Ekman pumping. During MAM, TIO SSTAs remain negative, although SSTAs begin to decay in the western TIO. Cold SSTAs play an active role in suppressing atmospheric convection, which decreases convective heating response, thus reducing wind anomalies (Fig. 9b).

We infer that the low-level Gill-type circulation shown in Fig. 8a is associated with diabatic heating in the central-eastern TIO, where the highest SSTs are located (>28°C). Corresponding to higher Tibetan Plateau snow depth, negative OLR and positive precipitation anomalies occur over the central-eastern TIO at lags of one and two months (Fig. 10), indicating enhanced convection and release of latent heating. This convective-related latent heating is the likely driver of the Gill-type circulation favorable for cold SSTAs over the TIO, suggesting a passive response of TIO SSTAs to atmospheric convection. Significantly suppressed convection and negative precipitation anomalies also cover most of the western Pacific (Fig. 10). These atmospheric responses are consistent with a previous study by Lyu et al. (2018), who noted a possible linkage between convective activity over the Indo-Pacific and snow cover over the Tibetan Plateau.

Due to both albedo and hydrological effects (Yasunari et al. 1991), higher Tibetan Plateau snow depth can cool the air

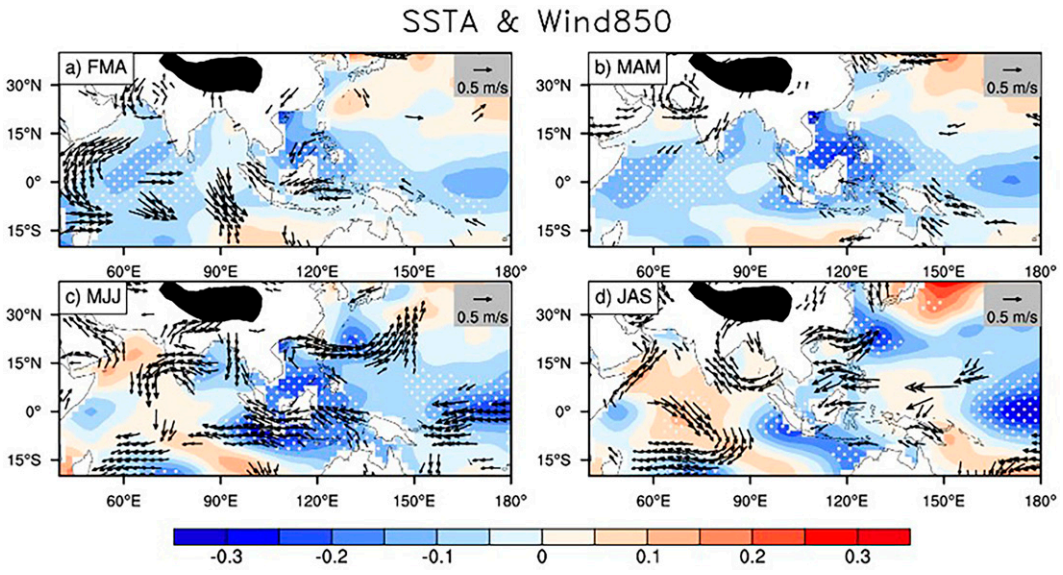

FIG. 9. Partial regression of (a) FMA, (b) MAM, (c) MJJ, and (d) JAS 850-hPa wind anomalies (vectors; m s^{-1}) and SSTAs (shading; °C) on the Tibetan Plateau snow depth index during 2000–14 with the Niño-3.4 index linearly removed. White dots and black arrows indicate regression coefficients that are significant at the 90% confidence level.

column from the surface throughout the troposphere, causing subsidence of isobaric surfaces over the Tibetan Plateau (Figs. 11c,d). With higher Tibetan Plateau snow depth, predominately negative geopotential height anomalies are located in the eastern Tibetan Plateau and propagate eastward in FMA (Figs. 11c,d). Consistent negative geopotential height anomalies and a corresponding anomalous cyclonic circulation at 200 hPa are found over the Tibetan Plateau, although JFM anomalies are not significant. Significant negative anomalies occur off of the coast of East Asia in FMA (Figs. 11a,b). Climatologically, the South Asia high is located in the western Pacific during winter–spring (Fig. 12) and shifts gradually westward while intensifying. The South Asia high remains over the Tibetan Plateau during the following summer due to sensible and monsoonal heating (Flohn 1957; Duan and Wu 2005). The eastward extension of geopotential height anomalies acts to displace the South Asia high.

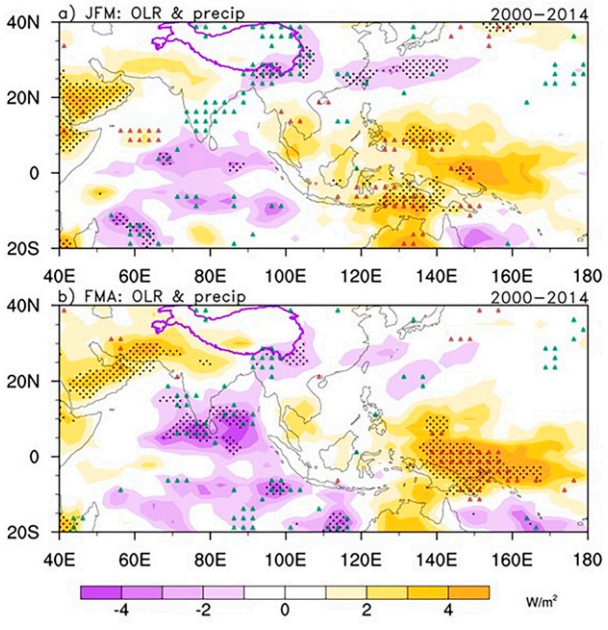

FIG. 10. Partial regression of (a) JFM and (b) FMA outgoing longwave radiation (shading; W m^{-2}) on the Tibetan Plateau snow depth index during 2000–14 with the Niño-3.4 index linearly removed. Black dots indicate regression coefficients that are significant at the 90% confidence level. Green (orange) triangles represent positive (negative) precipitation anomalies significant at the 90% confidence level.

As illustrated by Fig. 12, during increased Tibetan Plateau snow depth years (2005, 2008, 2012; values greater than 0.6), the center of the South Asia high (represented by the 12 470 gpm contour) is similar to climatology. However, the western ridge of the South Asia high extends westward near the Philippines during reduced Tibetan Plateau snow depth years (2001, 2009, 2013, 2014; values less than −0.6). In FMA, the ridge extends farther westward in reduced Tibetan Plateau snow depth years due to positive height anomalies to its west. The large extent of the South Asia high in FMA is favorable for anomalous convection through enhanced upper-level divergence. In contrast, suppressed convection is favored over the western Pacific during increased Tibetan Plateau snow depth years, further enhancing convection to its west via a compensatory effect, as suggested by Lyu et al. (2018) (Fig. 10). An anomalous zonal vertical circulation ultimately forms over the Indo-Pacific and releases anomalous latent heating driving a Gill-type circulation over the TIO. These atmospheric fields regressed against the Tibetan Plateau snow depth index are in agreement with the physical mechanism presented by Lyu et al. (2018).

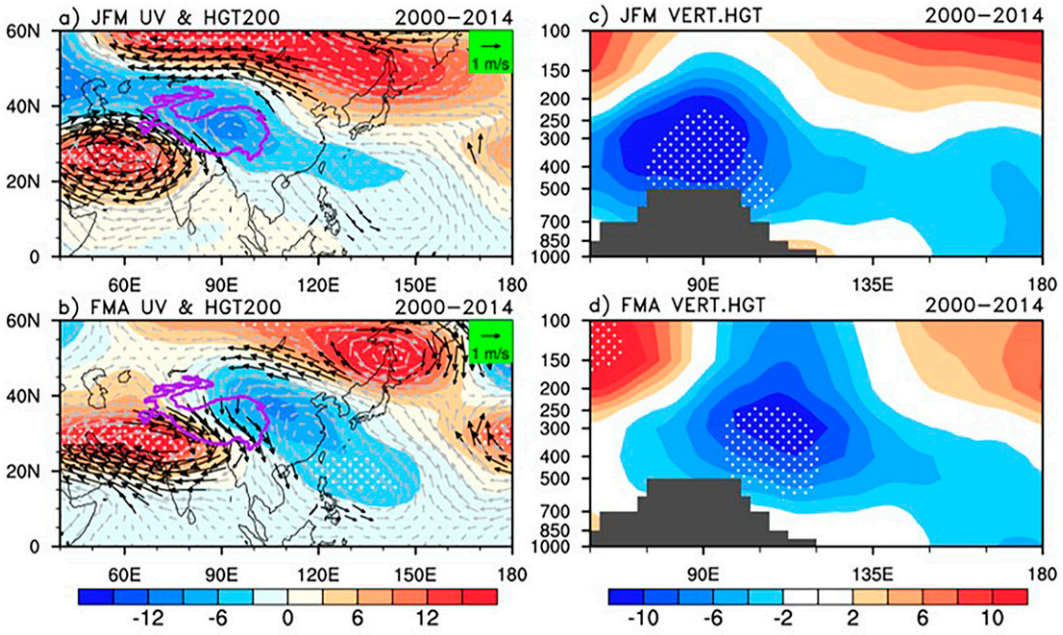

FIG. 11. Anomalies of 200-hPa geopotential height (shading; gpm) and wind (vector; m s^{-1}) in (a) JFM and (b) FMA obtained by partial regression onto the Tibetan Plateau snow depth index with the Niño-3.4 index linearly removed during 2000–14. (c), (d) As in (a) and (b), but for longitude–pressure cross sections of geopotential height along 35°N. White dots indicate values significant at the 90% confidence level. The gray shading represents topography.

Climatologically, the onset of the southwestern monsoon over the Bay of Bengal occurs in early May (Wu and Zhang 1998; Wang and LinHo 2002; Wu et al. 2012a; Shin and Huang 2016). Increased Tibetan Plateau snow can weaken the Asian monsoon through changes in Tibetan Plateau thermodynamic processes that decrease the land–sea thermal contrast (Zhang and Tao 2001; Kripalani et al. 2003; Zhao et al. 2007; You et al. 2020; Han et al. 2021). As shown in Fig. 9c, easterly anomalies

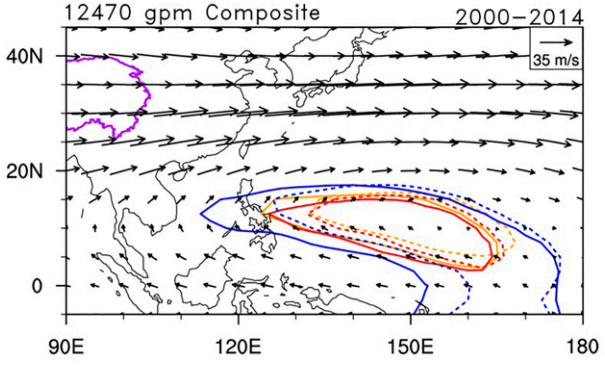

FIG. 12. Composite contours of 12 470 gpm at 200 hPa for high Tibetan Plateau snow depth years (red line), low Tibetan Plateau snow depth years (blue line), and average (yellow line) for 2000–14, overlying the averaged 200-hPa winds during 2000–14. Dashed (solid) lines denote contours in JFM (FMA). High (low) years refer to the standard deviation of the Tibetan Plateau snow depth index greater (lower) than 0.6 (−0.6).

over South Asia correspond to decreased monsoon intensity during the early monsoon season (MJJ) during 2000–14. When Tibetan Plateau snow depth is above normal, regressed wind anomalies oppose the prevailing southwest monsoon, reducing latent heating extracted from the ocean (Fig. S6), thus resulting in anomalous western TIO SST warming (Figs. 9c,d) due to the wind–evaporation–SST mechanism (Xie and Philander 1994).

Western TIO warm SSTAs gradually develop from MJJ through JAS (Figs. 9c,d). As noted by previous studies (Wu et al. 2008; Du et al. 2009), changes in latent heat fluxes are a key process in the TIO SST evolution. Downward latent heat fluxes cover the northern TIO in MJJ, extending south of the equator in JAS (Figs. S6a,b), largely due to a weakened monsoon circulation (Figs. 9c,d). The monsoon circulation is weakened by higher snow depth over the Tibetan Plateau due to changes in the land–sea thermal contrast. The zonal SST gradient over the TIO increases, thus driving low-level easterlies off of the coast of Sumatra (Lindzen and Nigam 1987) (Fig. 9c). The offshore winds near Sumatra further amplify the SST difference between the eastern and western TIO through both eastward transport of warm water and oceanic downwelling of a westward-propagating oceanic Rossby wave (Webster et al. 1999; Xie et al. 2002). Both processes strengthen warm western TIO SSTAs, especially south of the equator, consistent with prior studies (Xie et al. 2002; Du et al. 2009). The warming SSTAs have an asymmetric cross-equatorial distribution (Figs. 9c,d). As suggested by previous studies, asymmetric warm SSTAs favor a reversal in the Asian monsoon (Wu et al. 2008) and the occurrence of cyclonic anomalies over the

southwestern TIO (Fig. S6c) (Xie et al. 2002; Du et al. 2009). Corresponding to high snow depth over the Tibetan Plateau, negative summer precipitation anomalies occur in the northeastern Bay of Bengal (Fig. S6c), a key region for summer monsoon precipitation (He et al. 2023; T. Zhang et al. 2022), further confirming the weakened monsoon circulation response to higher Tibetan Plateau snow depth. Additionally, positive precipitation anomalies appear in the southwestern TIO, concurrent with anomalous cyclonic anomalies (Fig. S6c), highlighting the atmospheric response to convective heating (Gill 1980; Xie et al. 2002; Du et al. 2009). We do find northwesterly anomalies northeast of the anomalous cyclonic circulation, reducing low-level wind speeds and helping to persist warm SSTAs over the western TIO (Fig. S6).

We should caution that the evolution of TIO SST documented above only appears in the period from 2000 to 2014. During 1979–99, the responses of SSTAs and low-level wind anomalies in winter–spring to changes in Tibetan Plateau snow depth are weaker than during 2000–14 (Fig. S7). The observed significant OLR and precipitation anomalies associated with Tibetan Plateau snow depth generally occur over the Indo-Pacific in JFM during 1979–99 (Fig. S8). This response for the period from 1979 to 1999 almost disappears with a one-month lag, while the response intensifies with a one-month lag in 2000–14. Correspondingly, we find that the location of the convective pattern in 1979–99 is farther southward than in 2000–14 (Fig. S8a). The westward extension of the South Asia high in the Northern Hemisphere plays a lesser role in modulating convection south of the equator, leading to convective anomalies that tend to disappear quickly. Changes in the location of convection are possibly attributed to latitudinal shifts in the intertropical convergence zone (Fig. 13).

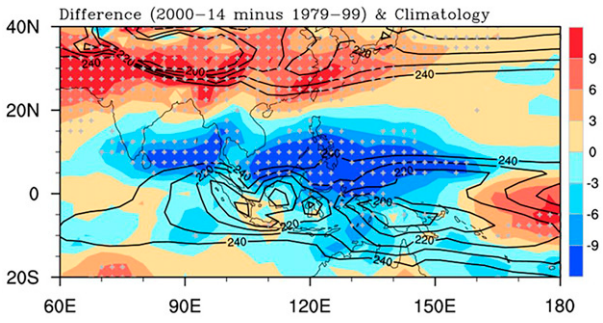

FIG. 13. Difference in outgoing longwave radiation (shading; W m^{-2}) in FMA between 2000–14 and 1979–99. The black contours indicate the climatological outgoing longwave radiation distribution averaged from 1979 to 2014. The plus signs indicate that the difference is significant at the 90% confidence level.

6. Summary and discussion

This study explores why there is a weak correlation between spring TIO SST and RITC frequency during the peak season from 2000 to 2014. During 2000–14, basinwide cold TIO SSTAs in spring are found to be closely associated with a Gill-type circulation that is excited by local convective-related latent heating, in response to higher Tibetan Plateau snow depth. Higher Tibetan Plateau snow depth results in a colder column of air along with negative geopotential heights in the troposphere over the Tibetan Plateau. This height pattern impacts the displacement of the upper-tropospheric South Asia high, with a weaker intensity and a smaller westward extension. This results in an anomalous zonal vertical circulation over the Indo-Pacific region and accompanying anomalous TIO ascent (Lyu et al. 2018). The released latent heating further excites a Gill-type circulation that cools SSTAs over the TIO via Ekman pumping (Fig. 14a).

During the following seasons, downward latent heating fluxes induced by the reversed monsoon circulation facilitate persistently warming SSTAs over the western TIO. Higher Tibetan Plateau snow depth tends to decrease monsoon intensity, leading to initially warming SSTAs in the western TIO through downward latent heat fluxes over the TIO (Xie and Philander 1994) during early summer. As the direct effect of the snow decays, the maintenance of downward latent heat fluxes is then supported by convective heating and a corresponding anomalous cyclone in the southwestern TIO (Fig. S6). Local air–sea interaction further extends the response of Tibetan Plateau snow depth, thus facilitating the formation of a positive IOD-like SST mode in JAS (right panel of Figs. 14b and 9d).

The warm SSTAs developing from spring through the peak season in the western TIO are closely related to Tibetan Plateau snow depth and determine the relationship between spring TIOB and RITC frequency. Local cold SSTAs can act to generate an anomalous cyclonic circulation via both an eastward-propagating Kelvin wave and an associated meridional-vertical circulation. Due to the strong impact of anomalously high Tibetan Plateau snow depth, significant warming SSTAs develop in the western TIO, generating a positive IOD-like SST mode during the TC peak season (right panel of Fig. 14b). The warm pool of SSTAs can excite an opposing Kelvin wave–related circulation that largely offsets the effect of the SSTA cold pool. On the other hand, higher Tibetan Plateau snow depth induces an anticyclonic circulation via the PMM over the WNP (Fig. 2a), possibly diminishing the cyclonic circulation excited by cold SSTAs in the eastern TIO and western Pacific. When the impact of Tibetan Plateau snow depth is linearly removed, warm SSTAs develop slowly and are smaller in magnitude compared with the impact of Tibetan Plateau snow depth included, likely indicating a limited role in modulating the WNP atmospheric circulation. We deduce that only cold SSTAs over the eastern TIO and western Pacific can act to excite a low-level cyclonic circulation that significantly increases RITC frequency (left panel of Fig. 14b). Large-scale factors (e.g., low-level relative vorticity, vertical motion) associated with the spring TIOB index support changes in RITC frequency.

In this study, we have explored the causes of the weak correlation between TIO SST and RITC frequency during the peak season of 2000–14 from the perspective of changes in Tibetan Plateau snow depth. However, during 1979–99, generally characterized by a positive PDO phase, there was an insignificant relationship between Tibetan Plateau snow depth

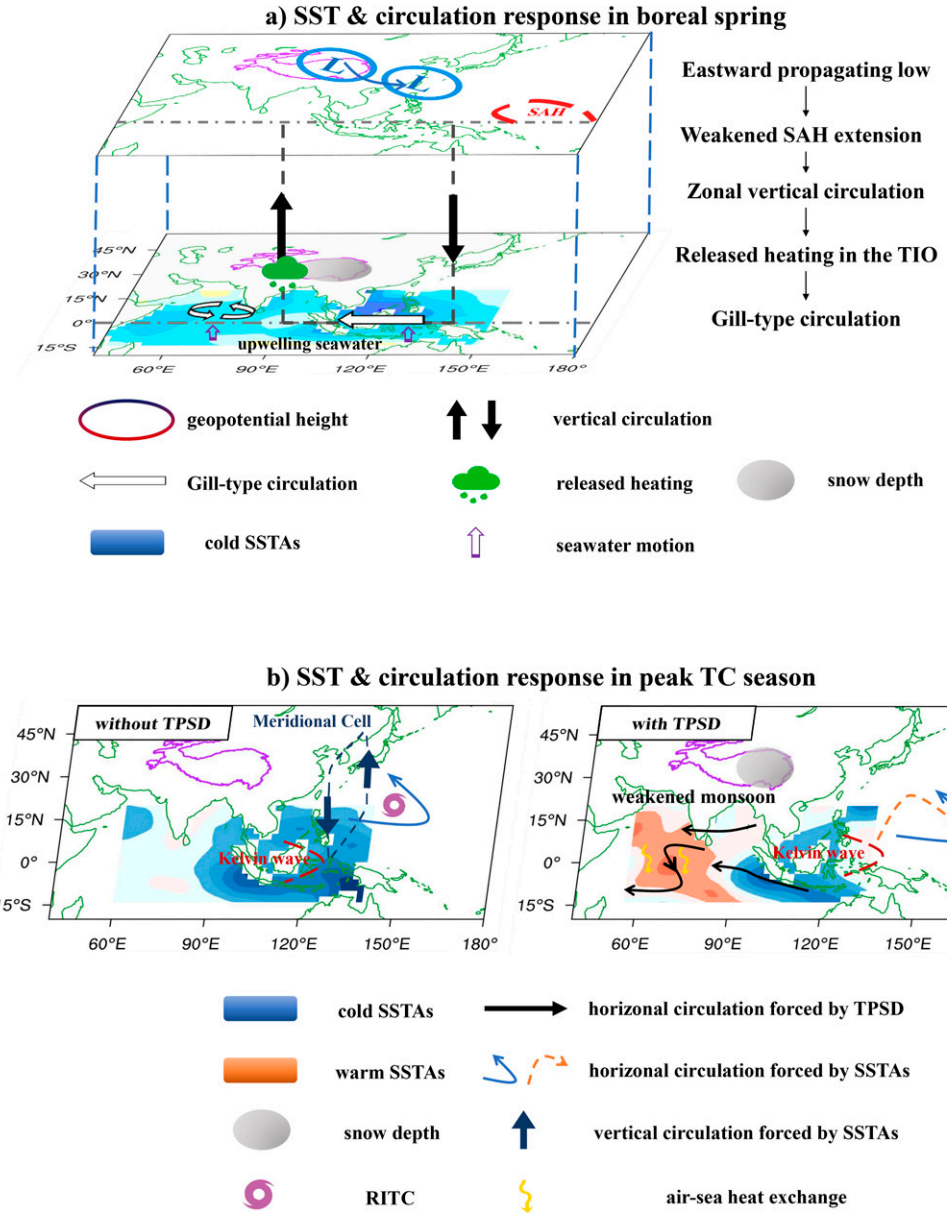

FIG. 14. Schematic diagram presenting the effect of winter–spring Tibetan Plateau snow depth thermal forcing on the evolution of Indo-Pacific SSTA and the circulation anomaly from spring to the peak season.

and RITCs (Fig. 1b) (Cai et al. 2022). Anomalous convection generally trended southward during this time period (Fig. S8, Fig. 12), likely resulting in little impact on spring TIO SST. After 2000, prevailing equatorial convection shifted northward.

We also note that the weak correlation between peak season TC genesis and spring TIO SST during 2000–14 becomes significant when the Tibetan Plateau snow depth signal is linearly removed. This indicates that changes in Tibetan Plateau snow depth should be considered when preseason TIO SST is employed as a predictor for peak-season TC counts. Nevertheless, we note that there are some discrepancies with results from previous studies on the simultaneous impact of TIO SST on WNP TCs (Zhan et al. 2011a, 2014), possibly due to changes in TC seasonality and changes on interdecadal time scales (Choi et al. 2019; Zhao and Wang 2019; Wu et al. 2021). The winter–spring atmospheric response to spring Tibetan Plateau snow depth (Figs. 9–11) is largely consistent with the simultaneous winter atmospheric response to Tibetan Plateau snow cover as shown by Lyu et al. (2018), but the one-month lagged response to winter–spring (JFM) Tibetan Plateau snow depth appears to be stronger. These results imply different climatic effects of snow cover and snow depth. The quantitative impacts of the snow cover and snow depth impacts on the large-scale circulation deserve an additional

study. The correlation between Tibetan Plateau snow depth and the principal component of SEOF indicates that there are additional climate variables contributing to the seasonal evolution of TIO SSTAs (Figs. 3 and 8), suggesting that the Tibetan Plateau snow depth is only one of many factors that influence the TIOB. Also, the specific physical mechanism on the evolution of TIO SST is not clearly identified due to the limitation of regression analysis, although we obtain a consistent atmospheric response to snow forcing over the Tibetan Plateau. Further investigations should be performed by using fully coupled (i.e., land–ocean–atmosphere) numerical model experiments to directly verify the response of TIO SSTAs to Tibetan Plateau snow depth.

This study has primarily focused on air–sea interactions over the Indo-Pacific region. The results of this study on the joint effect of Tibetan Plateau snow depth and TIO SST on RITCs may have important implications for seasonal forecasting of WNP RITCs. Although our study and several prior studies have highlighted the impact of Tibetan Plateau snow on the atmospheric and oceanic circulation, more detailed studies are needed to further investigate the proposed physical processes.

Acknowledgments. This research was jointly supported by the National Key R&D Program of China (2022YFF0801602) and the Natural Science Foundation of China (Grant 42192551) and the Six Talent Peaks project in Jiangsu Province (Grant JY-100). P. Klotzbach acknowledges a grant from the G. Unger Vetlesen Foundation. We acknowledge the High-Performance Computing Center of Nanjing University of Information Science and Technology for their support of this work. Observational snow-depth data are provided by the National Tibetan Plateau Data Center (http://data.tpdc.ac.cn).

Data availability statement. The TC best track data from JTWC are available at https://www.metoc.navy.mil/jtwc/jtwc.html?western-pacific. The National Centers for Environmental Prediction–Department of Energy AMIP-II Reanalysis data are available at https://psl.noaa.gov/data/gridded/data.ncep.reanalysis2.html. Monthly outgoing longwave radiation data from NOAA are available at https://www.psl.noaa.gov/data/gridded/data.interp_OLR.html. SST data from NOAA Extended Reconstructed SST V5 are available at https://www.ncei.noaa.gov/pub/data/cmb/ersst/v5/netcdf/. SODA version 3 monthly data can be obtained from https://dsrs.atmos.umd.edu/DATA/soda3.12.2/REGRIDED/ocean/. The PMM index can be downloaded at https://www.aos.wisc.edu/~dvimont/MModes/Data.html. Monthly snow-depth data in the study are obtained from GLDAS at https://disc.gsfc.nasa.gov/datasets?keywords=GLDAS. ERA5 data are available at https://cds.climate.copernicus.eu/cdsapp#!/dataset/reanalysis-era5-single-levels-monthly-means?tab=form. ERA-Interim data are available at https://apps.ecmwf.int/datasets/data/interim-full-daily/levtype=sfc/JRA-55 data are available at https://rda.ucar.edu/datasets/ds628.1/. The observation snow-depth data are provided by National Tibetan Plateau Data Center at https://data.tpdc.ac.cn/en/data/72d6dadf-8e1c-458b-b24e-91539042dfe6/.

REFERENCES

Adler, R. F., and Coauthors, 2018: The Global Precipitation Climatology Project (GPCP) Monthly analysis (new version 2.3) and a review of 2017 global precipitation. *Atmosphere*, **9**, 138, https://doi.org/10.3390/atmos9040138.

Ashok, K., S. K. Behera, S. A. Rao, H. Weng, and T. Yamagata, 2007: El Niño Modoki and its possible teleconnection. *J. Geophys. Res.*, **112**, C11007, https://doi.org/10.1029/2006JC003798.

Barnett, T. P., L. Dümenil, U. Schlese, E. Roeckner, and M. Latif, 1989: The effect of Eurasian snow cover on regional and global climate variations. *J. Atmos. Sci.*, **46**, 661–686, https://doi.org/10.1175/1520-0469(1989)046<0661:TEOESC>2.0.CO;2.

Blanford, H. F., 1884: On the connexion of the Himalaya snowfall with dry winds and seasons of drought in India. *Proc. Roy. Soc. London*, **37**, 3–22, https://doi.org/10.1098/rspl.1884.0003.

Brand, S., 1973: Rapid intensification and low-latitude weakening of tropical cyclones of the western North Pacific Ocean. *J. Appl. Meteor. Climatol.*, **12**, 94–103, https://doi.org/10.1175/1520-0450(1973)012<0094:RIALLW>2.0.CO;2.

Cai, Y., X. Han, H. Zhao, P. J. Klotzbach, L. Wu, G. B. Raga, and C. Wang, 2022: Enhanced predictability of rapidly intensifying tropical cyclones over the western North Pacific associated with snow depth changes over the Tibetan Plateau. *J. Climate*, **35**, 2093–2110, https://doi.org/10.1175/JCLI-D-21-0758.1.

Chen, R., Z. Wen, and R. Lu, 2018: Interdecadal change on the relationship between the mid-summer temperature in South China and atmospheric circulation and sea surface temperature. *Climate Dyn.*, **51**, 2113–2126, https://doi.org/10.1007/s00382-017-4002-5.

——, ——, ——, and C. Wang, 2019: Causes of the extreme hot midsummer in central and South China during 2017: Role of the western tropical Pacific warming. *Adv. Atmos. Sci.*, **36**, 465–478, https://doi.org/10.1007/s00376-018-8177-4.

Chiang, J. C. H., and D. J. Vimont, 2004: Analogous Pacific and Atlantic meridional modes of tropical atmosphere–ocean variability. *J. Climate*, **17**, 4143–4158, https://doi.org/10.1175/JCLI4953.1.

Choi, Y., K.-J. Ha, and F.-F. Jin, 2019: Seasonality and El Niño diversity in the relationship between ENSO and western North Pacific tropical cyclone activity. *J. Climate*, **32**, 8021–8045, https://doi.org/10.1175/JCLI-D-18-0736.1.

Chu, D., Q. Luosang, Z. Lin, and Y. Yang, 2018: Spatio-temporal variation of snow depth on Tibetan Plateau over the last 30 years (in Chinese with English abstract). *Meteor. Mon.*, **44**, 233–243.

Chu, J.-H., C. R. Sampson, A. S. Levine, and E. Fukada, 2002: The Joint Typhoon Warning Center tropical cyclone best-tracks, 1945–2000. Tech Rep. NRL/MR/7540-02-16, 22 pp., https://www.metoc.navy.mil/jtwc/products/best-tracks/tc-bt-report.html.

Craig, G. C., and S. L. Gray, 1996: CISK or WISHE as the mechanism for tropical cyclone intensification. *J. Atmos. Sci.*, **53**, 3528–3540, https://doi.org/10.1175/1520-0469(1996)053<3528:COWATM>2.0.CO;2.

Dee, D. P., and Coauthors, 2011: The ERA-Interim reanalysis: Configuration and performance of the data assimilation system. *Quart. J. Roy. Meteor. Soc.*, **137**, 553–597, https://doi.org/10.1002/qj.828.

DeMaria, M., C. R. Sampson, J. A. Knaff, and K. D. Musgrave, 2014: Is tropical cyclone intensity guidance improving? *Bull. Amer. Meteor. Soc.*, **95**, 387–398, https://doi.org/10.1175/BAMS-D-12-00240.1.

Ding, Y., 1992: Effects of the Qinghai-Xizang (Tibetan) Plateau on the circulation features over the plateau and its surrounding areas. *Adv. Atmos. Sci.*, **9**, 112–130, https://doi.org/10.1007/BF02656935.

Du, Y., S.-P. Xie, G. Huang, and K. Hu, 2009: Role of air–sea interaction in the long persistence of El Niño–induced north Indian Ocean warming. *J. Climate*, **22**, 2023–2038, https://doi.org/10.1175/2008JCLI2590.1.

——, L. Yang, and S.-P. Xie, 2011: Tropical Indian Ocean influence on northwest Pacific tropical cyclones in summer following strong El Niño. *J. Climate*, **24**, 315–322, https://doi.org/10.1175/2010JCLI3890.1.

Duan, A. M., and G. X. Wu, 2005: Role of the Tibetan Plateau thermal forcing in the summer climate patterns over subtropical Asia. *Climate Dyn.*, **24**, 793–807, https://doi.org/10.1007/s00382-004-0488-8.

Elsberry, R. L., T. D. B. Lambert, and M. A. Boothe, 2007: Accuracy of Atlantic and eastern North Pacific tropical cyclone intensity forecast guidance. *Wea. Forecasting*, **22**, 747–762, https://doi.org/10.1175/WAF1015.1.

Flohn, H., 1957: Large-scale aspects of the "summer monsoon" in South and East Asia. *J. Meteor. Soc. Japan*, **35A**, 180–186, https://doi.org/10.2151/jmsj1923.35A.0_180.

Gao, J., H. Zhao, P. J. Klotzbach, C. Wang, G. B. Raga, and S. Chen, 2020: Possible influence of tropical Indian Ocean sea surface temperature on the proportion of rapidly intensifying western North Pacific tropical cyclones during the extended boreal summer. *J. Climate*, **33**, 9129–9143, https://doi.org/10.1175/JCLI-D-20-0087.1.

Gao, S., L. Zhu, W. Zhang, and Z. Chen, 2018: Strong modulation of the Pacific meridional mode on the occurrence of intense tropical cyclones over the western North Pacific. *J. Climate*, **31**, 7739–7749, https://doi.org/10.1175/JCLI-D-17-0833.1.

Gill, A., 1980: Some simple solutions for heat-induced tropical circulation. *Quart. J. Roy. Meteor. Soc.*, **106**, 447–462, https://doi.org/10.1002/qj.49710644905.

Gray, W. M., 1975: Tropical cyclone genesis. Atmospheric Science Paper 234, Colorado State University, 121 pp.

Guo, Y.-P., and Z.-M. Tan, 2018: Westward migration of tropical cyclone rapid-intensification over the northwestern Pacific during short duration El Nino. *Nat. Commun.*, **9**, 1507, https://doi.org/10.1038/s41467-018-03945-y.

——, and ——, 2021: Influence of different ENSO types on tropical cyclone rapid intensification over the western North Pacific. *J. Geophys. Res. Atmos.*, **126**, e2020JD033059, https://doi.org/10.1029/2020JD033059.

Ha, Y., Z. Zhong, X. Yang, and Y. Sun, 2014: Contribution of east Indian Ocean SSTA to western North Pacific tropical cyclone activity under El Niño/La Niña conditions. *Int. J. Climatol.*, **35**, 506–519, https://doi.org/10.1002/joc.3997.

Han, X., H. Zhao, P. J. Klotzbach, L. Wu, and G. B. Raga, 2021: Impact of Tibetan Plateau snow cover on tropical cyclogenesis via the Madden–Julian oscillation during the following boreal summer. *Climate Dyn.*, **56**, 3025–3043, https://doi.org/10.1007/s00382-021-05625-y.

He, B., Y. Liu, G. Wu, Z. Wang, and Q. Bao, 2018: The role of air–sea interactions in regulating the thermal effect of the Tibetan–Iranian Plateau on the Asian summer monsoon. *Climate Dyn.*, **52**, 4227–4245, https://doi.org/10.1007/s00382-018-4377-y.

He, L., T. Zhou, and X. Chen, 2023: South Asian summer rainfall from CMIP3 to CMIP6 models: Biases and improvements. *Climate Dyn.*, https://doi.org/10.1007/s00382-022-06542-4, in press.

Hendricks, E. A., M. S. Peng, B. Fu, and T. Li, 2010: Quantifying environmental control on tropical cyclone intensity change. *Mon. Wea. Rev.*, **138**, 3243–3271, https://doi.org/10.1175/2010MWR3185.1.

Hersbach, H., and Coauthors, 2020: The ERA5 global reanalysis. *Quart. J. Roy. Meteor. Soc.*, **146**, 1999–2049, https://doi.org/10.1002/qj.3803.

Holliday, C. R., and A. H. Thompson, 1979: Climatological characteristics of rapidly intensifying typhoons. *Mon. Wea. Rev.*, **107**, 1022–1034, https://doi.org/10.1175/1520-0493(1979)107<1022:CCORIT>2.0.CO;2.

Hsu, P.-C., P.-S. Chu, H. Murakami, and X. Zhao, 2014: An abrupt decrease in the late-season typhoon activity over the western North Pacific. *J. Climate*, **27**, 4296–4312, https://doi.org/10.1175/JCLI-D-13-00417.1.

Huang, B., and Coauthors, 2017: Extended Reconstructed Sea Surface Temperature, version 5 (ERSSTv5): Upgrades, validations, and intercomparisons. *J. Climate*, **30**, 8179–8205, https://doi.org/10.1175/JCLI-D-16-0836.1.

Huangfu, J., W. Chen, R. Huang, and J. Feng, 2019: Modulation of the impacts of the Indian Ocean basin mode on tropical cyclones over the northwest Pacific during the boreal summer by La Niña Modoki. *J. Climate*, **32**, 3313–3326, https://doi.org/10.1175/JCLI-D-18-0638.1.

Hurrell, J. W., and Coauthors, 2013: The Community Earth System Model: A framework for collaborative research. *Bull. Amer. Meteor. Soc.*, **94**, 1339–1360, https://doi.org/10.1175/BAMS-D-12-00121.1.

Kanamitsu, M., W. Ebisuzaki, J. Woollen, S.-K. Yang, H. M. Fiorion, and G. L. Potter, 2002: NCEP–DOE AMIP-II Reanalysis (R-2). *Bull. Amer. Meteor. Soc.*, **83**, 1631–1644, https://doi.org/10.1175/BAMS-83-11-1631.

Kaplan, J., and M. DeMaria, 2003: Large-scale characteristics of rapidly intensifying tropical cyclones in the North Atlantic basin. *Wea. Forecasting*, **18**, 1093–1108, https://doi.org/10.1175/1520-0434(2003)018<1093:LCORIT>2.0.CO;2.

——, and Coauthors, 2015: Evaluating environmental impacts on tropical cyclone rapid intensification predictability utilizing statistical models. *Wea. Forecasting*, **30**, 1374–1396, https://doi.org/10.1175/WAF-D-15-0032.1.

Klein, S. A., B. J. Soden, and N.-C. Lau, 1999: Remote sea surface temperature variations during ENSO: Evidence for a tropical atmospheric bridge. *J. Climate*, **12**, 917–932, https://doi.org/10.1175/1520-0442(1999)012<0917:RSSTVD>2.0.CO;2.

Kobayashi, S., and Coauthors, 2015: The JRA-55 reanalysis: General specifications and basic characteristics. *J. Meteor. Soc. Japan*, **93**, 5–48, https://doi.org/10.2151/jmsj.2015-001.

Kripalani, R. H., A. Kulkarni, and S. S. Sabade, 2003: Western Himalayan snow cover and Indian monsoon rainfall: A re-examination with INSAT and NCEP/NCAR data. *Theor. Appl. Climatol.*, **74** (1–2), 1–18, https://doi.org/10.1007/s00704-002-0699-z.

Lee, C.-Y., M. K. Tippett, A. H. Sobel, and S. J. Camargo, 2016: Rapid intensification and the bimodal distribution of tropical cyclone intensity. *Nat. Commun.*, **7**, 10625, https://doi.org/10.1038/ncomms10625.

Li, G., J. Lu, B. Jin, and N. Bu, 2001: The effects of anomalous snow cover of the Tibetan Plateau on the surface heating. *Adv. Atmos. Sci.*, **18**, 1207–1214, https://doi.org/10.1007/s00376-001-0034-0.

Li, W., W. Guo, B. Qiu, Y. Xue, P.-C. Hsu, and J. Wei, 2018: Influence of Tibetan Plateau snow cover on East Asian atmospheric circulation at medium-range time scales. *Nat. Commun.*, **9**, 4243, https://doi.org/10.1038/s41467-018-06762-5.

Liebmann, B., and A. Smith, 1996: Description of a complete (interpolated) outgoing longwave radiation dataset. *Bull. Amer. Meteor. Soc.*, **77**, 1275–1277, https://doi.org/10.1175/1520-0477-77.6.1274.

Lin, H., and Z. Wu, 2011: Contribution of the autumn Tibetan Plateau snow cover to seasonal prediction of North American winter temperature. *J. Climate*, **24**, 2801–2813, https://doi.org/10.1175/2010JCLI3889.1.

Lindzen, R. S., and S. Nigam, 1987: On the role of sea surface temperature gradients in forcing low-level winds and convergence in the tropics. *J. Atmos. Sci.*, **44**, 2418–2436, https://doi.org/10.1175/1520-0469(1987)044<2418:OTROSS>2.0.CO;2.

Liu, C., W. Zhang, F. Jiang, M. F. Stuecker, and Z. Huang, 2021: Record-low WNP tropical cyclone activity in early summer 2020 due to Indian Ocean warming and Madden-Julian Oscillation activity. *Geophys. Res. Lett.*, **48**, e2021GL094578, https://doi.org/10.1029/2021GL094578.

Liu, G., R. Wu, Y. Zhang, and S. Nan, 2014: The summer snow cover anomaly over the Tibetan Plateau and its association with simultaneous precipitation over the mei-yu-baiu region. *Adv. Atmos. Sci.*, **31**, 755–764, https://doi.org/10.1007/s00376-013-3183-z.

Liu, K. S., and J. C. L. Chan, 2013: Inactive period of western North Pacific tropical cyclone activity in 1998–2011. *J. Climate*, **26**, 2614–2630, https://doi.org/10.1175/JCLI-D-12-00053.1.

Liu, S., Q. Wu, S. R. Schroeder, Y. Yao, Y. Zhang, T. Wu, L. Wang, and H. Hu, 2020: Near-global atmospheric responses to observed springtime Tibetan Plateau snow anomalies. *J. Climate*, **33**, 1691–1706, https://doi.org/10.1175/JCLI-D-19-0229.1.

Liu, Y., P. Huang, and G. Chen, 2019: Impacts of the combined modes of the tropical Indo-Pacific Sea surface temperature anomalies on the tropical cyclone genesis over the western North Pacific. *Int. J. Climatol.*, **39**, 2108–2119, https://doi.org/10.1002/joc.5938.

——, M. Lu, H. Yang, A. Duan, B. He, S. Yang, and G. Wu, 2020: Land–atmosphere–ocean coupling associated with the Tibetan Plateau and its climate impacts. *Natl. Sci. Rev.*, **7**, 534–552, https://doi.org/10.1093/nsr/nwaa011.

Lu, M., S. Yang, Z. Li, B. He, S. He, and Z. Wang, 2018: Possible effect of the Tibetan plateau on the "upstream" climate over west Asia, north Africa, south Europe and the north Atlantic. *Climate Dyn.*, **51**, 1485–1498, https://doi.org/10.1007/s00382-017-3966-5.

Lu, Y., H. Zhao, D. Zhao, and Q. Li, 2021: Spatial-temporal characteristic of tropical cyclone disasters in China during 1984–2017 (in Chinese with English abstract). *Haiyang Xuebao*, **43**, 45–61.

Lyu, M., M. Wen, and Z. Wu, 2018: Possible contribution of the inter-annual Tibetan Plateau snow cover variation to the Madden–Julian oscillation convection variability. *Int. J. Climatol.*, **38**, 3787–3800, https://doi.org/10.1002/joc.5533.

National Meteorological Information Center, and Tibet Meteorological Bureau, 2018: Observational snow depth dataset of the Tibetan Plateau (version 1.0) (1961–2013). National Tibetan Plateau/Third Pole Environment Data Center, accessed 17 August 2022, https://doi.org/10.11888/Snow.tpdc.270558.

Neale, R. B., and Coauthors, 2010: Description of the NCAR Community Atmosphere Model (CAM5.0). NCAR Tech. Note NCAR/TN-486+STR, 268 pp.

North, G. R., T. L. Bell, R. F. Cahalan, and F. J. Moeng, 1982: Sampling errors in the estimation of empirical orthogonal functions. *Mon. Wea. Rev.*, **110**, 699–706, https://doi.org/10.1175/1520-0493(1982)110<0699:SEITEO>2.0.CO;2.

Orsolini, Y., and Coauthors, 2019: Evaluation of snow depth and snow cover over the Tibetan Plateau in global reanalyses using in situ and satellite remote sensing observations. *Cryosphere*, **13**, 2221–2239, https://doi.org/10.5194/tc-13-2221-2019.

Ose, T., 1996: The comparison of the simulated response to the regional snow mass anomalies over Tibet, Eastern Europe, and Siberia. *J. Meteor. Soc. Japan*, **74**, 845–866, https://doi.org/10.2151/jmsj1965.74.6_845.

Pradhan, P. K., B. Preethi, K. Ashok, R. Krishnan, and A. K. Sahai, 2011: Modoki, Indian Ocean dipole, and western North Pacific typhoons: Possible implications for extreme events. *J. Geophys. Res.*, **116**, D18108, https://doi.org/10.1029/2011JD015666.

Qian, Q., X. Jia, and R. Wu, 2019: Changes in the impact of the autumn Tibetan Plateau snow cover on the winter temperature over North America in the mid-1990s. *J. Geophys. Res. Atmos.*, **124**, 10 321–10 343, https://doi.org/10.1029/2019JD030245.

Rappaport, E. N., and Coauthors, 2009: Advances and challenges at the National Hurricane Center. *Wea. Forecasting*, **24**, 395–419, https://doi.org/10.1175/2008WAF2222128.1.

Rodell, M., and Coauthors, 2004: The Global Land Data Assimilation System. *Bull. Amer. Meteor. Soc.*, **85**, 381–394, https://doi.org/10.1175/BAMS-85-3-381.

Saji, N. H., B. N. Goswami, P. N. Vinayachandran, and T. Yamagata, 1999: A dipole mode in the tropical Indian Ocean. *Nature*, **401**, 360–363, https://doi.org/10.1038/43854.

Schreck, C. J., K. R. Knapp, and J. P. Kossin, 2014: The impact of best track discrepancies on global tropical cyclone climatologies using IBTrACS. *Mon. Wea. Rev.*, **142**, 3881–3899, https://doi.org/10.1175/MWR-D-14-00021.1.

Shi, D., X. Ge, M. Peng, and T. Li, 2019: Characterization of tropical cyclone rapid intensification under two types of El Niño events in the western North Pacific. *Int. J. Climatol.*, **40**, 2359–2372, https://doi.org/10.1002/joc.6338.

Shin, C.-S., and B. Huang, 2016: Slow and fast annual cycles of the Asian summer monsoon in the NCEP CFSv2. *Climate Dyn.*, **47**, 529–553, https://doi.org/10.1007/s00382-015-2854-0.

Shinoda, T., Y. Morinaga, and T. Yasunari, 2003: The forefront of monsoon researches (in Japanese). *Kisho Kenkyu Notes*, **204**, 69–114.

Si, D., and Y. Ding, 2013: Decadal change in the correlation pattern between the Tibetan Plateau winter snow and the East Asian summer precipitation during 1979–2011. *J. Climate*, **26**, 7622–7634, https://doi.org/10.1175/JCLI-D-12-00587.1.

Song, J., Y. Duan, and P. J. Klotzbach, 2020: Increasing trend in rapid intensification magnitude of tropical cyclones over the western North Pacific. *Environ. Res. Lett.*, **15**, 084043, https://doi.org/10.1088/1748-9326/ab9140.

Sun, R., A. Duan, L. Chen, and Y. Li, 2019: Interannual variability of the North Pacific mixed layer associated with the spring Tibetan Plateau thermal forcing. *J. Climate*, **32**, 3109–3130, https://doi.org/10.1175/JCLI-D-18-0577.1.

Turner, A. G., and J. M. Slingo, 2011: Using idealized snow forcing to test teleconnections with the Indian summer monsoon in the Hadley Centre GCM. *Climate Dyn.*, **36**, 1717–1735, https://doi.org/10.1007/s00382-010-0805-3.

Ventham, J. D., and B. Wang, 2007: Large-scale flow patterns and their influence on the intensification rates of western North

Pacific tropical storms. *Mon. Wea. Rev.*, **135**, 1110–1127, https://doi.org/10.1175/MWR3327.1.

Wahiduzzaman, M., and A. Yeasmin, 2019: Statistical forecasting of tropical cyclone landfall activities over the North Indian Ocean rim countries. *Atmos. Res.*, **227**, 89–100, https://doi.org/10.1016/j.atmosres.2019.04.034.

——, K. Cheung, J.-J. Luo, P. K. Bhaskaran, S. Tang, and C. Yuan, 2022: Impact assessment of Indian Ocean dipole on the North Indian Ocean tropical cyclone prediction using a statistical model. *Climate Dyn.*, **58**, 1275–1292, https://doi.org/10.1007/s00382-021-05960-0.

Wang, B., and LinHo, 2002: Rainy season of the Asian–Pacific summer monsoon. *J. Climate*, **15**, 386–398, https://doi.org/10.1175/1520-0442(2002)015<0386:RSOTAP>2.0.CO;2.

——, and S.-I. An, 2005: A method for detecting season-dependent modes of climate variability: S-EOF analysis. *Geophys. Res. Lett.*, **32**, L15710, https://doi.org/10.1029/2005GL022709.

——, and X. Zhou, 2008: Climate variation and prediction of rapid intensification in tropical cyclones in the western North Pacific. *Meteor. Atmos. Phys.*, **99**, 1–16, https://doi.org/10.1007/s00703-006-0238-z.

——, Q. Bao, B. Hoskins, G. Wu, and Y. Liu, 2008: Tibetan Plateau warming and precipitation changes in East Asia. *Geophys. Res. Lett.*, **35**, L14702, https://doi.org/10.1029/2008GL034330.

Wang, C., K. Wu, L. Wu, H. Zhao, and J. Cao, 2021: What caused the unprecedented absence of western North Pacific tropical cyclones in July 2020? *Geophys. Res. Lett.*, **48**, e2020GL092282, https://doi.org/10.1029/2020GL092282.

Wang, Chenghai, K. Yang, Y. Li, D. Wu, and Y. Bo, 2017: Impacts of spatiotemporal anomalies of Tibetan Plateau snow cover on summer precipitation in eastern China. *J. Climate*, **30**, 885–903, https://doi.org/10.1175/JCLI-D-16-0041.1.

Wang, Chunzai, X. Wang, R. H. Weisberg, and M. L. Black, 2017: Variability of tropical cyclone rapid intensification in the North Atlantic and its relationship with climate variations. *Climate Dyn.*, **49**, 3627–3645, https://doi.org/10.1007/s00382-017-3537-9.

Wang, X., and H. Liu, 2016: PDO modulation of ENSO effect on tropical cyclone rapid intensification in the western North Pacific. *Climate Dyn.*, **46**, 15–28, https://doi.org/10.1007/s00382-015-2563-8.

——, C. Wang, L. Zhang, and X. Wang, 2015: Multidecadal variability of tropical cyclone rapid intensification in the western North Pacific. *J. Climate*, **28**, 3806–3820, https://doi.org/10.1175/JCLI-D-14-00400.1.

Wang, Z., A. Duan, and S. Yang, 2019: Potential regulation on the climatic effect of Tibetan Plateau heating by tropical air–sea coupling in regional models. *Climate Dyn.*, **52**, 1685–1694, https://doi.org/10.1007/s00382-018-4218-z.

——, R. Wu, A. Duan, and X. Qu, 2020: Influence of eastern Tibetan Plateau spring snow cover on North American air temperature and its interdecadal change. *J. Climate*, **33**, 5123–5139, https://doi.org/10.1175/JCLI-D-19-0455.1.

——, ——, S. Yang, and M. Lu, 2022: An interdecadal change in the influence of ENSO on the spring Tibetan Plateau snow-cover variability in the early 2000s. *J. Climate*, **35**, 725–743, https://doi.org/10.1175/JCLI-D-21-0348.1.

Webster, P. J., A. M. Moore, J. P. Loschnigg, and R. R. Leben, 1999: Coupled ocean–atmosphere dynamics in the Indian Ocean during 1997–98. *Nature*, **401**, 356–360, https://doi.org/10.1038/43848.

Wu, G., and Y. Zhang, 1998: Tibetan Plateau forcing and the timing of the monsoon onset over South Asia and the South China Sea. *Mon. Wea. Rev.*, **126**, 913–927, https://doi.org/10.1175/1520-0493(1998)126<0913:TPFATT>2.0.CO;2.

——, and Coauthors, 1997: Sensible heat driven air-pump over the Tibetan Plateau and its impacts on the Asian summer monsoon. *Collections on the Memory of Zhao Jiuzhang*, Y. Duzheng, Ed., Chinese Science Press, 116–126.

——, and Coauthors, 2007: The influence of mechanical and thermal forcing by the Tibetan Plateau on Asian climate. *J. Hydrometeor.*, **8**, 770–789, https://doi.org/10.1175/JHM609.1.

——, Y. Guan, Y. Liu, J. Yan, and J. Mao, 2012a: Air–sea interaction and formation of the Asian summer monsoon onset vortex over the Bay of Bengal. *Climate Dyn.*, **38**, 261–279, https://doi.org/10.1007/s00382-010-0978-9.

——, Y. Liu, B. He, Q. Bao, A. Duan, and F.-F. Jin, 2012b: Thermal controls on the Asian summer monsoon. *Sci. Rep.*, **2**, 404, https://doi.org/10.1038/srep00404.

Wu, R., B. P. Kirtman, and V. Krishnamurthy, 2008: An asymmetric mode of tropical Indian Ocean rainfall variability in boreal spring. *J. Geophys. Res.*, **113**, D05104, https://doi.org/10.1029/2007JD009316.

——, X. Cao, and Y. Yang, 2020: Interdecadal change in the relationship of the western North Pacific tropical cyclogenesis frequency to tropical Indian and North Atlantic Ocean SST in early 1990s. *J. Geophys. Res. Atmos.*, **125**, e2019JD031493, https://doi.org/10.1029/2019JD031493.

Wu, Z., C. Hu, J. Wang, W. Chen, T. Lian, S. Yang, and D. Chen, 2021: Distinct interdecadal change contrasts between summer and autumn in latitude–longitude covariability of northwest Pacific typhoon genesis locations. *Geophys. Res. Lett.*, **48**, e2021GL093494, https://doi.org/10.1029/2021GL093494.

Xiao, Z., and A. Duan, 2016: Impacts of Tibetan Plateau snow cover on the interannual variability of the East Asian summer monsoon. *J. Climate*, **29**, 8495–8514, https://doi.org/10.1175/JCLI-D-16-0029.1.

Xie, L., and T. Yan, 2007: West North Pacific typhoon track patterns and their potential connection to Tibetan Plateau snow cover. *Nat. Hazards*, **42**, 317–333, https://doi.org/10.1007/s11069-006-9087-9.

——, ——, L. J. Pietrafesa, T. Karl, and X. Xu, 2005: Relationship between western North Pacific typhoon activity and Tibetan Plateau winter and spring snow cover. *Geophys. Res. Lett.*, **32**, L16703, https://doi.org/10.1029/2005GL023237.

Xie, S.-P., and S. G. H. Philander, 1994: A coupled ocean–atmosphere model of relevance to the ITCZ in the eastern Pacific. *Tellus*, **46A**, 340–350, https://doi.org/10.3402/tellusa.v46i4.15484.

——, H. Annamalai, F. A. Schott, and J. P. McCreary, 2002: Structure and mechanisms of South Indian Ocean climate variability. *J. Climate*, **15**, 864–878, https://doi.org/10.1175/1520-0442(2002)015<0864:SAMOSI>2.0.CO;2.

——, T. Sampe, G. Huang, Y. Du, H. Tokinaga, J. Hafner, and K. Hu, 2009: Indian Ocean capacitor effect on Indo–western Pacific climate during the summer following El Niño. *J. Climate*, **22**, 730–747, https://doi.org/10.1175/2008JCLI2544.1.

Yanai, M., L. Changfeng, and Z. Song, 1992: Seasonal heating of the Tibetan Plateau and its effects on the evolution of the Asian summer monsoon. *J. Meteor. Soc. Japan*, **70**, 319–351, https://doi.org/10.2151/jmsj1965.70.1B_319.

Yasunari, T., A. Kitoh, and T. Tokioka, 1991: Local and remote responses to excessive snow mass over Eurasia appearing in the northern spring and summer climate—A study with the

MRI·GCM. *J. Meteor. Soc. Japan*, **69**, 473–487, https://doi.org/10.2151/jmsj1965.69.4_473.

You, Q., and Coauthors, 2020: Review of snow cover variation over the Tibetan Plateau and its influence on the broad climate system. *Earth-Sci. Rev.*, **201**, 103043, https://doi.org/10.1016/j.earscirev.2019.103043.

Yu, L., and D. Hu, 2008: Role of snow depth in spring of Tibetan Plateau in onset of South China Sea summer monsoon (in Chinese with English abstract). *Chin. J. Geophys.*, **51**, 1682–1694.

Yuan, J., and J. Cao, 2013: North Indian Ocean tropical cyclone activities influenced by the Indian Ocean dipole mode. *Sci. China Earth Sci.*, **56**, 855–865, https://doi.org/10.1007/s11430-012-4559-0.

Zhan, R., Y. Wang, and X. Lei, 2011a: Contributions of ENSO and east Indian Ocean SSTA to the interannual variability of northwest Pacific tropical cyclone frequency. *J. Climate*, **24**, 509–521, https://doi.org/10.1175/2010JCLI3808.1.

——, ——, and C.-C. Wu, 2011b: Impact of SSTA in the east Indian Ocean on the frequency of northwest Pacific tropical cyclones: A regional atmospheric model study. *J. Climate*, **24**, 6227–6242, https://doi.org/10.1175/JCLI-D-10-05014.1.

——, ——, and L. Tao, 2014: Intensified impact of East Indian Ocean SST anomaly on tropical cyclone genesis frequency over the western North Pacific. *J. Climate*, **27**, 8724–8739, https://doi.org/10.1175/JCLI-D-14-00119.1.

——, Y. Ding, L. Wu, and X. Lei, 2016: Role of ENSO in the interannual relationship between Tibetan Plateau winter snow cover and northwest Pacific tropical cyclone genesis frequency. *Sci. China Earth Sci.*, **59**, 2009–2021, https://doi.org/10.1007/s11430-015-5559-y.

Zhang, M., D. Jin, X. Wang, L. Chen, J. Luo, and Z. Wang, 2022: Seasonal transition of precedent Indian Ocean basin mode and subsequent Indian Ocean dipole without El Niño–Southern Oscillation impact. *Int. J. Climatol.*, **42**, 9023–9031, https://doi.org/10.1002/joc.7793.

Zhang, Q., L. Wu, and Q. Liu, 2009: Tropical cyclone damages in China. *Bull. Amer. Meteor. Soc.*, **90**, 489–496, https://doi.org/10.1175/2008BAMS2631.1.

Zhang, S., and S. Tao, 2001: Influence of snow cover over the Tibetan Plateau on Asian summer monsoon (in Chinese with English abstract). *Chin. J. Atmos. Sci.*, **25**, 372–390.

Zhang, T., X. Jiang, S. Yang, J. Chen, and Z. Li, 2022: A predictable prospect of the South Asian summer monsoon. *Nat. Commun.*, **13**, 7080, https://doi.org/10.1038/s41467-022-34881-7.

Zhang, Y., T. Li, and B. Wang, 2004: Decadal change of the spring snow depth over the Tibetan Plateau: The associated circulation and influence on the East Asian summer monsoon. *J. Climate*, **17**, 2780–2793, https://doi.org/10.1175/1520-0442(2004)017<2780:DCOTSS>2.0.CO;2.

Zhao, H., and C. Wang, 2016: Interdecadal modulation on the relationship between ENSO and typhoon activity during the late season in the western North Pacific. *Climate Dyn.*, **47**, 315–328, https://doi.org/10.1007/s00382-015-2837-1.

——, and ——, 2019: On the relationship between ENSO and tropical cyclones in the western North Pacific during the boreal summer. *Climate Dyn.*, **52**, 275–288, https://doi.org/10.1007/s00382-018-4136-0.

——, X. Duan, G. B. Raga, and P. J. Klotzbach, 2018: Changes in characteristics of rapidly intensifying western North Pacific tropical cyclones related to climate regime shifts. *J. Climate*, **31**, 8163–8179, https://doi.org/10.1175/JCLI-D-18-0029.1.

——, Y. Lu, Y., X. Jiang, P. J. Klotzbach, L. Wu, and J. Cao, 2022: A statistical intraseasonal prediction model of extended boreal summer western North Pacific tropical cyclone genesis. *J. Climate*, **35**, 2459–2478, https://doi.org/10.1175/JCLI-D-21-0110.1.

Zhao, P., Z. Zhou, and J. Liu, 2007: Variability of Tibetan spring snow and its associations with the hemispheric extratropical circulation and East Asian summer monsoon rainfall: An observational investigation. *J. Climate*, **20**, 3942–3955, https://doi.org/10.1175/JCLI4205.1.

Zhao, Y., A. Duan, and G. Wu, 2021: Opposite responses of the Indian Ocean to the thermal forcing of the Tibetan Plateau before and after the onset of the South Asian monsoon. *J. Climate*, **34**, 8389–8408, https://doi.org/10.1175/JCLI-D-20-0982.1.

Zhou, Q., L. Wei, and R. Zhang, 2019: Influence of Indian Ocean dipole on tropical cyclone activity over western North Pacific in boreal autumn. *J. Ocean Univ. China*, **18**, 795–802, https://doi.org/10.1007/s11802-019-3965-8.

Zhu, Y., H. Liu, Y. Ding, F. Zhang, and W. Li, 2015: Interdecadal variation of spring snow depth over the Tibetan Plateau and its influence on summer rainfall over East China in the recent 30 years. *Int. J. Climatol.*, **35**, 3654–3660, https://doi.org/10.1002/joc.4239.